A Highly Efficient, Low-Cost, and Sustainable Method of Water Purification and Desalination Using Solar-Driven Interfacial Evaporation

by

Esther Uchechukwu Nnaeme

Submitted in fulfillment of the academic requirements of

Master of Science

in Chemistry

School of Chemistry and Physics

College of Agriculture, Engineering and Science

University of Kwazulu-Natal

South Africa

February, 2024

Preface

A dissertation completed by the candidate and submitted to the School of Chemistry and Physics, College of Agriculture, Engineering and Science, University of KwaZulu-Natal, Westville, for the degree of Master of Science.

The contents of this work have not been submitted in any form to another University and, except where the work of others is acknowledged in the text, the results reported were duly carried out by the candidate.

Signed: Prof. Werner Van Zyl

Main Supervisor

Date: 30 January 2024

Signed: Dr. Ajay Bissessur

Co-supervisor

Date: 05-02-2024

Declaration: Plagiarism

1. I, Esther Uchechukwu Nnaeme, understand that plagiarism is to use another's work and present it as my own, and that this is a criminal offence.

2. Each significant contribution and quotation in this research from the work(s) of other people has been attributed and has been cited as such.

3. This research, "A Highly Efficient, Low-Cost, and Sustainable Method of Water Purification and Desalination Using Solar-Driven Interfacial Evaporation", is my work.

Student no: 222045966

Signed: Esther Uchechukwu Nnaeme Date: 5th February, 2024.

Abstract

Water scarcity has become one of the most daunting global challenges, and as a result, a continuous supply of potable water has become a bane to most societies. Techniques such as distillation and reverse osmosis have been adopted in the production of potable water but these processes are energy-consuming and highly expensive making them less attractive to many households. A viable economical technique is the removal of salt from seawater or brackish water through a solar distiller.

This research was based on the design of a low-cost and new improved solar distiller which was made up of a wooden basin and an inclined glass cover. In the basin is contained sea or brackish water and photothermal materials which include recycled materials that act as an insulation material, an evaporation structure, and a solar absorber. These photothermal materials were designed and fabricated to meet with the current state-of-the-art method of evaporation which is solar interfacial evaporation. The fabricated materials were characterized using scanning electron microscopy (SEM), and Fourier transform infrared spectroscopy (FTIR). The solar distiller and photo thermal materials were evaluated for their efficiencies via real-time outdoor experiments using solar energy. The rate of evaporation was calculated, while parameters such as pH, conductivity, Total dissolved solids (TDS) and salinity were analyzed on the freshwater collected and compared with the standard of drinking water by the World Health Organisation (WHO) and South African National Standard (SANS241). Heavy metal concentration in the water samples and remediated water collected were analyzed using inductively coupled plasma optical emission spectroscopy (ICP-OES) and compared with the WHO and SANS241 standards as well.

The findings could provide adequate and affordable potable water to all households irrespective of societal status and it will reduce the cost of health management, as many diseases associated with consumption of untreated water can be drastically reduced. This is in-line with South Africa's National Development Plan (NDP) 2030 and the United Nations' Sustainable Development Goals (SDGs).

Conference Participation

1. **Esther Nnaeme**, Werner E. Van Zyl, Ajay Bissessur, *A highly efficient, low-cost, and sustainable method of water purification and desalination using solar-driven interfacial evaporation.* (Flash presentation at the Postgraduate Research and Innovation Symposium held at Coastlands hotel, Musgrave, Durban on the 3rd November, 2023). 3rd prize winner.

Acknowledgments

My profound gratitude goes to God Almighty, for his guidance, good health, protection, wisdom and for allowing me to get to this height.

I am most grateful to my supervisors, Prof. Werner Van Zyl and Dr. Ajay Bissessur, for their mentorship, support, and for taking me through an interesting approach of research. I could not have done this without your guidance and I must say you are the best supervisors I could ever ask for.

To my parents, Dr. & Mrs. Francis Okafor and my adorable siblings, I could not have come this far without your prayers, good wishes and encouragements. I love you all.

I am forever grateful to my colleagues: Mr. Isaac, Taiwo Aderemi, Gedeon, Omoye, Dr. Elizabeth, Mr. Jeremiah, Monadia, Emmanuel, and Mary for helping me in their unique ways and making this journey an exciting one.

On a special note, I would like to thank The University of KwaZulu-Natal, for giving me the opportunity to pursue my MSc degree in this University. The School of Chemistry and Physics for bench space and instruments, and the entire staff starting from the store department (Mr. Gregory and Mr. Shanon), the technical team (Ms. Anita and Unathi), Mr Mbuso Cele (the designer of the solar still), Mr. Frank, the Academics most especially Prof. Van Zyl, Dr. Bissessur, Prof. Olatunji, and Dr. C. Koorbanally.

Most especially, my heartfelt gratitude goes to my husband, Dr. C.C. Nnaeme for his encouragement, motivations, moral and financial support, prayers, love, and understanding while I was studying and conducting my research. It is with a feeling of immense accomplishment that I dedicate this dissertation to you my darling husband.

List of Abbrevations

ALP	Air Laid Paper
CSIR	Council for Scientific and Industrial Research
EBT	Eriochrome Black T
EC	Electrical Conductivity
ED	Electrodialysis
EDR	Electrodialysis Reversal
EDTA	Ethylenediaminetetraacetic acid
EPS	Expanded Polystyrene
EVA	Ethylene vinyl acetate
FO	Forward Osmosis
FTIR	Fourier Transform Infrared
GO	Graphene Oxide
HDH	Humidification-dehumidification
MD	Membrane Distillation
MED	Multi-effect Distillation
MF	Microfiltration
MSF	Multi-stage Flash
NDP	National Development Plan
NF	Nanofiltration
PVA	Poly Vinyl Alcohol
RO	Reverse Osmosis
SANS	South African National Standards

SDG	Sustainable Development Goals
SEM	Scanning Electron Microscopy
SS	Solar Still
STD	Standard
TDS	Total dissolved solids
VCD	Vapour Compression Distillation
VD	Vacuum Distillation
WHO	World Health Organisation

Table of Contents

List of Tables

List of Figures

Chapter 1

Introduction

1.1 General overview

Water is generally known as a universal solvent and is the most critical element to sustain life. Water is crucial to both plants and animals because without water, life becomes impossible. Water is used for drinking, domestic, industrial, agricultural, and recreational purposes. Water seems readily available, but how much of it can be described as potable is the challenge. Sources of water include seawater, rainwater, groundwater, polar ice caps, lake water, ocean water, river water, and atmospheric water vapor. Water can be classified into saline water, brackish water, and freshwater. As shown in Figure 1.1, about 96.5% of the total water on earth is salt water and 2.5% is freshwater, of which about 1.3% of the freshwater is locked up as glaciers and ice caps (Gleick, 1993) and over time, this has led to the scarcity of clean and freshwater.

The United Nations (UN) Sustainable Development Goals (SDGs) number 6 seeks to attain "clean water and sanitation" as a response to the potable water challenge globally. This goal has a target of providing clean, safe, and potable water for all. Its main objective is to ensure the availability and sustainable management of water for all by 2030 (United Nations, 2015). As a result, researchers are contributing tirelessly to the solution of global water crisis (WHO 2023). Water has become a scarce resource around the world with about 2.1 billion people lacking access to clean and safe drinking water and 3.4 million people dying every year as a result of drinking from contaminated water sources (WHO, 2023). Two-third of the world's population is facing the challenge of water shortage with about 71% living under moderate to severe scarcity while about 66% live under severe scarcity (Mekonnen & Hoekstra, 2016).

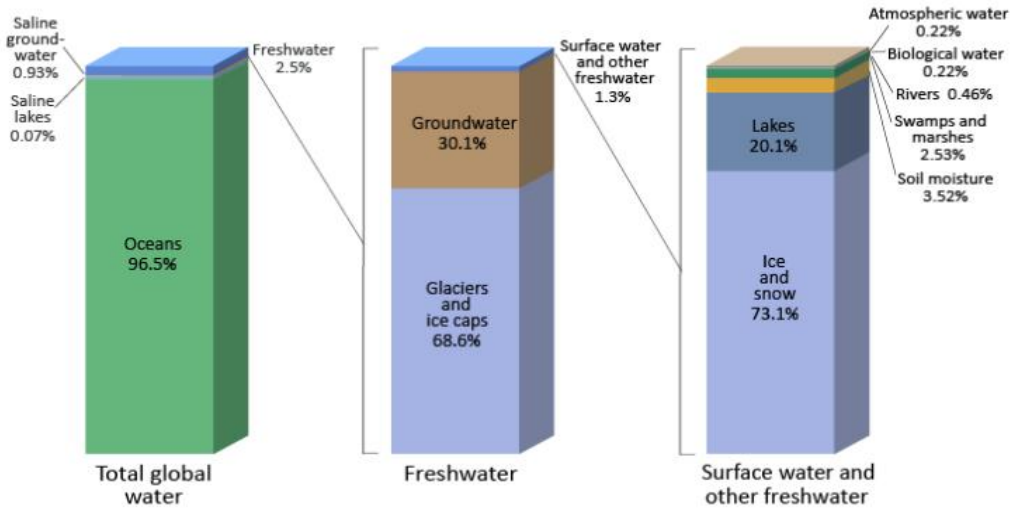

Figure 1.1: Distribution of Earth's water (Gleick, 1993)

The increase in population, as well as rapid development in the agricultural and industrial sectors, has led to the massive shortage and demand for freshwater all over the world (Aljubouri, 2017). As the population increases, the demand for water increases. The increase in water demand has exceeded the increase in the world's population and this is as a result of increasing domestic, agricultural and industrial demands (Mohammadi et al., 2019). Water scarcity could be as a result of high population density, practice of extreme irrigation agriculture or as a result of low natural water availability as experienced in arid regions (Mekonnen & Hoekstra, 2016).

Seawater is a mixture of 96.5% water and 3.5% different salts, organic and undissolved substances. Seawater has a pH ranging from 7.90 to 8.20. The density of seawater is about 1027 kg/m^3 which is greater than the density of pure water and this is a result of the salts contained in it increasing the salinity. The presence of the salt in seawater affects its temperature, density, compressibility, and freezing point but does not determine them. Hence, the saltier the water, the denser it becomes. The average seawater salinity is about 35%. Seawater contains the six most abundant ions chloride, sulphate, calcium, potassium, sodium, and magnesium (Balasubramanian, 2011).

The word brackish was coined from the Dutch root "brak" which means salty. Brackish water can be found in deltas of rivers, estuaries, lagoons and backwaters. They contain 0.5 – 30 g of salt per liter which can also be expressed as 0.5 – 30 parts per thousand (ppt or %). The salinity of brackish water depends on the tide, the amount of freshwater entering from rivers

as rain, and the rate of evaporation. Brackish waters are too saline to be potable but are less saline than seawater. Its TDS ranges from 1000 – 20000 mg/L (Drever, 1997).

The unavailability of freshwater has led to the discovery of techniques that convert seawater and brackish water into freshwater. Water treatment or purification is the removal or reduction of contaminants or undesirable elements in water to improve its quality and make it fit for its end-use such as drinking, domestic activities, irrigation, recreational, and industrial purposes. There are numerous water purification techniques and devices that are capable of converting impure water including saline water into freshwater fit for drinking of which desalination is one of them. Desalination, also known as desalting, is the process of removing salts, minerals and other contaminants from seawater, brackish water, and wastewater effluent in order to collect freshwater for consumption, industrial and domestic uses (Asadollahi et al., 2017).

There are various desalination techniques and each of them produces freshwater from sea or brackish water (Buros, 2000). The idea and improvement of desalination technologies have helped to produce more freshwater in different parts of the world, particularly in arid regions with intense shortages of freshwater and this has been a solution to collect freshwater for consumption, agricultural, industrial and domestic purposes.

The process of desalination can be performed through phase change (evaporation and condensation), or by the use of semi-permeable membrane, or by combining the two methods, each of these separates freshwater from saline water (Alnaimat et al., 2018).

Solar energy is an abundant source of renewable energy capable of solving many challenges, one of which is desalination. Solar desalination is a process that involves the evaporation of a saline solution (seawater or brackish water) utilising solar energy (energy from the sun) which then leads to condensation of the generated vapor which is collected as freshwater. Solar desalination has been proven to be low energy consuming and cost-effective and this is a huge advantage to areas suffering from clean water shortage and lack of electricity. Solar desalination provides a promising solution to produce clean water using the solar energy for rural areas and developing countries (Sharon & Reddy, 2015).

Solar desalination can be categorised into direct and indirect method. Direct solar desalination is a process where the solar energy is absorbed directly by the saline water and caused to evaporate after being heated up while indirect solar desalination is a process whereby the solar energy is absorbed by a solar collector before being transferred to the

saline water. A typical example of direct solar desalination is the solar still while the indirect solar desalination can be seen in humidification-dehumidification (Alnaimat et al., 2018).

Desalination can be classified into two broad technologies, which are thermal and membrane desalination. Thermal desalination technology is a process where the saline water is heated and the condensed vapour is collected as pure water. Thermal desalination technologies include: multi-stage flash distillation (MSF), Multi-effect distillation (MED), and Vapour compression distillation (VCD). In MSF, water vapour is generated by heating saline water, after which a drop in pressure occurs and water flashes to vapour. This process is carried out repeatedly in a series of chambers under reduced pressure at each stage. Water vapour is then condensed on a heat exchanger bundle and is collected as freshwater, but this flash distillation process is very expensive (Alnaimat et al., 2018).

In MED, the process takes place in a series of vessels called effects (temperature decreases as the effects move from stage to stage). The saline water is boiled through a series of effects and forms vapour that is collected as the distillate (Khan et al., 2021). MED uses less energy than MSF and does not require pretreatment of the saline water.

In VCD, the vapour is compressed and the latent heat of vapourisation is used to evaporate the polluted water. It is easy to operate, consumes less energy and can be operated without the need of external heat source (Shatilla, 2020). In VCD, the pressure of the saline water is decreased which causes it to boil at a lower temperature. The water is also evaporated, condensed and collected as freshwater (Essa et al., 2022).

HDH is also based on evaporation and condensation. Its working principle is based on the fact that vapour is contained in the air and the amount of vapour carried is proportional to the temperature of the air (Morris & Hanbury, 1991).

Membrane desalination technologies involve the use of a selective barrier to purify water. This include reverse osmosis (RO), forward osmosis (FO), microfiltration (MF), nanofiltration (NF), electrodialysis (ED), membrane distillation (MD), electrodialysis reversal (EDR) and gas separation.

In RO, saline water is made to pass through a semi-permeable membrane that allows only the freshwater pass through, leaving the concentrated saline water behind. This is by far the most seawater-to-drinking water conversion desalination process worldwide and can produce large volumes per day. It remains the most used technology for ion removal from brackish waters

(Liu et al., 2021). FO is combined with RO and also uses a semi-permeable membrane to purify water.

MF is also a pressure driven process. It is known to be capable of removing arsenic and other toxicities in water (Han et al., 2002). NF is used in waste water treatment. It has a pore size of 1 nm and is effective in the removal of bacteria, metals, and toxic chemicals (Essa et al., 2022).

ED is an expensive technique. It separates anions and cations from the water through the use of high electrical potential energy (Khan et al., 2018). Through this, salt particles are separated from freshwater by being forced out through a membrane.

MD eliminates non-volatile contaminants from the targeted water (González et al., 2017).

These methods of desalination have negative impacts on the environment in that they are energy intensive process and as a result, there can be gas emissions which can be harmful to both human beings and environment, in addition to the costs involved for installation and maintenance. Solar desalination has proven to be cost-effective, environment-friendly, and a sustainable method of collecting freshwater from saline water. Solar desalination is also the best remedy for arid regions and rural areas with very high solar intensity (Anaimat, 2011).

Evaporation is a process by which a liquid substance is converted into vapour. It is a surface phenomenon that occurs on the surface of a liquid (that is the boundary between the liquid and gaseous phase) as it changes into the gas phase. The rate of evaporation can be influenced by factors such as the concentration of the given molecules in the air, the temperature of the liquid, and the rate of airflow. Evaporation occurs when the partial pressure of the vapour of a substance is less than the equilibrium vapour pressure. It can happen in two ways, namely: by decreasing the air pressure, and by increasing the temperature of the water. When the temperature of water reaches its boiling point, vapourization takes place. Evaporation will continue to occur provided that there is sufficient heat and the vapour is unsaturated (Liu & Song, 2018). Evaporation can be useful in the separation of water from dissolved content, hence it is used for obtaining pure water or extracting valuable dissolved species like lithium salts (Ducker, 2023).

Condensation is a process by which water in its gas form (vapour) is turned into liquid. For condensation to occur, evaporation must first occur to generate vapour, and there must be

another object on where the vapour condenses. As the water saturated air that was caused by evaporation comes in contact with a cooler surface, condensation occurs.

1.2 Statement of the Problem

The issue of water scarcity globally increases everyday as the world's population increases. The increase in demand for freshwater is a result of agricultural activities, industrial activities, and urbanization. The World Health Organisation points out access to clean water as the most important global crisis of the 21st century as about 2.1 billion people in the world still lack access to clean and safe drinking water, and 3.4 million people die every year as a result of drinking from contaminated water sources (WHO, 2023).

Innovations and modern techniques of converting the available water in seas, oceans, lakes, estuaries etc., into freshwater have brought us this far, but these technologies are expensive and cannot be afforded by some societies, particularly in rural areas in developing countries. These technologies are very efficient in water treatment and purification but because most people around the world cannot afford them, it remains a challenge. It is in this regard that new, efficient, cost-effective, and sustainable methods of desalination must be discovered and developed in order to meet with the demands of supplying clean and potable water to all, and that was the topic of this study.

1.3 Hypothesis

Desalination through the use of a solar still and interfacial evaporation is a sustainable method of water purification as it is cost-effective and highly efficient in purifying water.

1.4 Aim and Objectives

This study aims to design a sustainable, green, and cost-effective method of water desalination using solar-driven interfacial evaporation. To realise this, the following objectives were set to guide the research:

1. To design and construct a low-cost and efficient solar still for water purification and desalination, paying close attention to the materials used, preferably being recyclable and bio-available.
2. To advance the throughput volume of the solar still and subsequent output volume of freshwater.
3. To analyze the remediated water obtained from the still.

1.5 Scope of the Study

The problem of water scarcity remains a global issue as the population and demand for freshwater increases. This research is targeted at providing a sustainable and cost-effective method of purifying water by solar desalination using a constructed still.

The experiments would be carried out during the winter season (July - August) and summer season (Sep - Nov) of the year 2023. This would be carried out in Durban, Kwazulu Natal province of South Africa. Four water samples would be used which include seawater sourced from South beach in Durban, synthetic water analytically prepared in the laboratory, tap water sourced from the rooftop of the H block, University of Kwazulu Natal, and borehole water sourced from a farm in Shongweni, Durban.

On these water samples, physicochemical parameters such as pH, conductivity, total dissolved solids, and salinity would be analysed before and after desalination. Hardness test using titration method would also be carried out on the water samples before and after desalination. The concentration of five metals which include Ca^{2+}, Fe^{3+}, Mg^{2+}, Na^{+}, and K^{+} present in the water samples before and after desalination would also be analysed using ICP-OES (Perkin Elmer Optima 5300 DV).

In order to improve the productivity and yield of the solar still, the state-of-the-art approach of evaporation which is solar-driven interfacial evaporation would be experimented on, and a design using pure cellulose and polystyrene in the construction of an evaporation structure would be made. A solar absorber and a wicking structure would be made from the pure cellulose, while the insulation material would be expanded polystyrene. These designed materials would be characterised using Scanning Electron Microscopy (SEM) and Fourier Transform Infrared Spectroscopy (FTIR).

This research would prove that solar-driven interfacial evaporation is the current state-of-the-art approach to improving the yield of a solar still by providing more quantity of freshwater, rather than using the conventional solar still that yields only a little amount of freshwater.

1.6 Layout of the Dissertation

This dissertation is made up of five chapters briefly described below.

Chapter 1 is the introductory part which describes the general overview of water shortage, its causes and some viable solutions. It also contains the statement of the problem and hypothesis of this research alongside the aim and objectives of study.

Chapter 2 covers the literature review of solar interfacial evaporation being a suitable method of desalination. The process of desalination and its different techniques are discussed. The concept of a solar still is illustrated and described outlining its advantages over the actual desalination plants. Factors that affect the efficiency of a solar still are also discussed. The concept of solar interfacial evaporation is illustrated and explained outlining the components of a photothermal material and how it aids interfacial evaporation and improves the yield of a solar still.

Chapter 3 is a detailed report of all the experiments, analysis, tests, and characterisation methods carried out in this research. The design of the solar still, the sourcing of every material used, and the methods of preparation were explained in detail.

Chapter 4 presents and discusses the findings which demonstrate that the remediated water collected from the solar still meets the requirements of a potable water.

Chapter 5 is the conclusions and recommendations for implementation and future research.

References

Aljubouri, A. A. (2017). Design and Manufacturing of Single Sloped Solar Still: Study the Effect of Inclination Angle and Water Depth on Still Performance. *Journal of Al-Nahrain University-Science*, *20*(2), 60–70. https://doi.org/10.22401/juns.20.2.08

Alnaimat, F., Klausner, J., Matthew, B. (2018). Solar desalination. In *Desalination and water treatment* (pp. 128–150). intechopen. https://doi.org/http:\\dx.doi.org\10.5772\intechopen.76981

Alnaimat, F. (2011). *Transient analysis of solar diffusion driven desalination*. University of Florida.

Asadollahi, M., Bastani, D., & Musavi, S. A. (2017). Enhancement of surface properties and performance of reverse osmosis membranes after surface modification: A review. *Desalination*, *420*(May), 330–383. https://doi.org/10.1016/j.desal.2017.05.027

Balasubramanian, A. (2011). *Properties of Seawater-Documentary*. https://doi.org/10.13140/RG.2.2.14014.48969

Buros, O. K. (2000). The ABCs of Desalting. *International Desalination Association* (2nd ed.). Topsfield, Massachusetts, USA.

Drever, J. (1997). *The Geochemistry of Natural Water: Surface and Groundwater Environments* (3rd ed.). Prentice Hall, New Jersey.

Ducker, W. A. (2023). Decreasing the Energy of Evaporation Using Interfacial Water: Is This Useful for Solar Evaporation Efficiency? [Research-article]. *ACS Omega*, *8*(22), 19705–19707. https://doi.org/10.1021/acsomega.3c01300

Essa, F. A., Abdullah, A. K., Majdi, H. S., Basem, A., Dhahad, H. A., Omara, Z. M., Mohammed, S. A., Alawee, W. H., Ezzi, A. Al, & Yusaf, T. (2022). Parameters Affecting the Efficiency of Solar Stills—Recent Review. *Sustainability (Switzerland)*, *14*(17). https://doi.org/10.3390/su141710668

Gleick, P. H. (1993). *Water in Crisis: A guide to the World's Freshwater Resources. Chapter 2.* Oxford University Press (pp. 13–23).

González, D., Amigo, J., & Suárez, F. (2017). Membrane distillation: Perspectives for sustainable and improved desalination. *Renewable and Sustainable Energy Reviews*,

80(April 2016), 238–259. https://doi.org/10.1016/j.rser.2017.05.078

Han, B., Runnellsb, T., Zimbronb, J., & Wickramasinghe, R. (2002). Arsenic removal from drinking water microfiltration. *Desalination*, *145*, 293–298. www.elsevier.com/locate/desal

Khan, Q., Maraqa, M., Mohamed, A. (2021). Chapter 17- Inland desalination: techniques, brine management, and environmental concerns. *Pollution Assessment for Sustainable Practices in Applied Sciences and Engineering*, 871–918. https://doi.org/https://doi.org/10.1016/B978-0-12-809582-9.00017-7

Khan, S. U. D., Danish, S. N., Orfi, J., Rana, U. A., & Haider, S. (2018). Nuclear Energy Powered Seawater Desalination. In *Renewable Energy Powered Desalination Handbook: Application and Thermodynamics*. Elsevier Inc. https://doi.org/10.1016/B978-0-12-815244-7.00006-4

Liu, X., Shanbhag, S., Bartholomew, T. V., Whitacre, J. F., & Mauter, M. S. (2021). Cost Comparison of Capacitive Deionization and Reverse Osmosis for Brackish Water Desalination. *ACS ES&T Engineering*, *1*(2), 261–273. https://doi.org/10.1021/acsestengg.0c00094

Liu, Y., & Song, C. (2018). Bioinspired Materials in Evaporation. *Bioinspired Engineering of Thermal Materials*, 73–98. https://doi.org/10.1002/9783527687596.ch4

Mekonnen, M. M., & Hoekstra, A. Y. (2016). Sustainability: Four billion people facing severe water scarcity. *Science Advances*, *2*(2), 1–7. https://doi.org/10.1126/sciadv.1500323

Mohammadi, K., Saghafifar, M., Ellingwood, K., & Powell, K. (2019). Hybrid concentrated solar power (CSP)-desalination systems: A review. *Desalination*, *468*(July), 114083. https://doi.org/10.1016/j.desal.2019.114083

Morris, R.M., Hanbury, W. T. (1991). Predication of critical desalination parameters using radial basis functions network. In *Proceedings of the new technologies for the use of renewable energy sources in water desalination.* (pp. 30–50).

Sharon, H., & Reddy, K. S. (2015). A review of solar energy driven desalination technologies. *Renewable and Sustainable Energy Reviews*, *41*, 1080–1118. https://doi.org/10.1016/j.rser.2014.09.002

Shatilla, Y. (2020). Nuclear desalination. In *Nuclear reactor technology development and utilization* (pp. 247–270). Elsevier Ltd. https://doi.org/https://doi.org/10.1016/C2018-0-04201-2.

United Nations. (2015). Transforming our world: the 2030 agenda for sustainable development. Washington DC. 21252030 Agenda for Sustainable Development web.pdf (un.org).

WHO. (2023). *Water is a basic human need*. Geneva. https://wholives.org/our-mission/mission/#.

Chapter 2

Literature Review: Solar Interfacial Evaporation – A Sustainable Method of Desalination

2.1 Desalination

Desalination is the process of removing dissolved mineral salts and unwanted organic matter from water. It is one of the most popular and viable methods of obtaining freshwater from sea and brackish water. Water obtained from desalination can be used for drinking, industrial, and agricultural purposes. The process of desalination has been a source of relief to the global water crisis. As the world's population increases, the demand for freshwater increases as well, with desalination being one of the major solutions to water shortage and scarcity.

There are approximately 16000 desalination plants spread across 177 countries which generate about 95 million m^3/day of freshwater (Jones et al., 2019). Australia, being an arid country, was the first country to adopt the process of desalination due to the reduced rainfall and drought experienced between 1997-2009 which was called the millennium drought. As of 2014, 35% of Israel's drinking water was provided by desalination, and in the year 2015, it was increased to 50% and expected to be 70% by 2050 (Kershner, 2015).

Countries in the Middle East such as Saudi Arabia, United Arab Emirates, Qatar, Kuwait, Bahrain, Oman, etc. depend highly on desalination with Saudi Arabia topping the list followed by The United Arab Emirates. Figures 2.1 and 2.2 show a desalination plant in Saudi Arabia.

Quite a number of challenges are associated with desalination such as being expensive and its high consumption of energy and land space. Another big issue is the discharge of highly concentrated wastewater (brine). This byproduct of desalination is usually discharged into the sea and ends up posing a great threat to aquatic life. Researchers around the world are working to find ways of developing more affordable and sustainable methods of desalination and ways in which the brine can be properly disposed of or reused.

Figure 2.1: Desalination plant in Saudi Arabia (Utilities middle east, 2018)

Figure 2.2: Desalination plant in Dubai (Kelsey, 2017).

Desalination plants are classified into two categories based on their mode of operation which are: thermal desalination and membrane desalination. Thermal desalination heats saline water and generates pure water by condensation while membrane desalination uses a semi-permeable membrane to separate clean water from contaminants.

2.1.1 Membrane Techniques

A membrane is a semipermeable or selective barrier that allows matter to pass through and refuse others from passing through and this is as a result of differences in size. For the purpose of desalination, membrane technology can be used to produce clean water from sea and brackish water and for industrial effluent treatment. (Tofighy et al., 2021). Some of the membrane processes include reverse osmosis (RO), forward osmosis, microfiltration (MF), nanofiltration (NF), electrodialysis (ED), membrane distillation (MD), electrodialysis reversal (EDR) and gas separation. Membrane technologies are used on large scales because they can filter polluted water with various sizes of contaminants (Zhao et al., 2020).

2.1.2 Reverse Osmosis

Osmosis is a process by which molecules of a solvent pass through a semipermeable membrane from a region of low concentration solution to a region of a higher concentration.

The reverse osmosis technique follows the basis of osmosis by forcing pressure higher than the osmotic pressure such that the freshwater molecules pass through the membrane while leaving the highly concentrated saline water behind at the other end of the membrane. Feed water is delivered under pressure through the semi permeable membrane, where water permeates the minute pores of the membrane and is delivered as purified water called permeate water (Garud et al., 2011). RO remains the most used technology for ion removal from brackish waters (Liu et al., 2021). RO units can be used in the purification of brackish water and seawater because they can filter the salt concentrations $\leq$45,000 ppm. Also, RO requires an energy amount proportion to the salt concentration of the feed water (Essa et al., 2022).

2.1.3 Forward Osmosis

In the forward osmosis process, two solutions with different concentrations are separated by a semi-permeable membrane. The concentrated solution is called “draw” while the diluted solution is called “feed” (Bajraktari et al., 2016). Unlike other water purification processes, the product of forward osmosis is not clean water and needs to be combined with a second step such as reverse osmosis to get clean water (Johnson et al., 2017).

2.1.4. Microfiltration (MF)

Microfiltration is a pressure-driven process of separation that is broadly used in the concentration, purification, or separation of macromolecules, suspended particles, and colloids from a solution (Charcosset, 2012).

Microfiltration is one of the most used techniques in municipal wastewater management, elimination of contamination from drinking water, and toxic industrial waste effluent treatment (Han et al., 2002). Research explored the removal of arsenic using microfiltration and flocculation and it was concluded that microfiltration of the flocculated water leads to low turbidity and arsenic removal in the filtrate. MF gained momentum in its application after the cryptosporidium outbreak in the United States in 1992, and in 2000, desalination industries commenced using MF as an advanced system for pre-treatment during seawater desalination to reduce the fouling process in the RO unit (Bardhan et al., 2022).

2.1.5 Nanofiltration

Nanofiltration is also a pressure-driven separation technique used for desalination and waste water treatment which possesses a pore size of 1 nm and and suitable for contaminants with a molecular weight of 100–1000 Da. It is effective in the removal of inorganic salts and organic pollutants from wastewater (Jakhar et al., 2023).

NF membranes are used for brackish water treatment, groundwater treatment, surface water treatment, water reuse, and point of use applications, and it is efficient in the removal of major pollutants (e.g., hardness, pathogen, and natural organic matter) and micro pollutants of major concern (e.g., disinfection of byproducts, per- and polyfluoroalkyl substances, and arsenic) (Guo et al., 2022). NF is the most reliable and effective technology among the pressure-driven membrane technologies for filtering undesired contaminated agents such as bacteria, metals, high TDS, and toxic chemicals (Essa et al., 2022).

2.1.6 Electrodialysis (ED)

ED is a process that uses charge selective membranes for the purpose of desalination. It separates anions and cations from the stream by using the high electrical potential energy which forces the salt particles to move through a membrane and then leave behind freshwater as the product (Khan et al., 2018). According to scientific, industrial and commercial reports, electrodialysis and electrodialysis reversal are more effective for purifying brackish water with TDS $\leq$ 35,000 ppm but the main limitation of both methods is that they are expensive (Essa et al., 2022).

2.1.7 Membrane Distillation (MD)

MD is used in desalination to remove non-volatile contaminants from the targeted water. In MD, a high-quality distillate is collected when the vapor from an aqueous solution crosses a microporous hydrophobic membrane and then condenses at the other side of the membrane. This process yields a highly pure distillate solution and a highly concentrated feed solution that contains the non-volatile solutes (González et al., 2017).

2.2 Thermal Distillation Techniques

Distillation is one of the oldest methods of water treatment. The concept behind this process is that water is heated to release vapour which is then condensed and collected as freshwater or the purest form of water. The thermal distillation techniques can be classified into direct and indirect thermal techniques (Essa et al., 2022). While direct thermal distillation techniques include humidification-dehumidification (HDH) and solar still units, indirect thermal distillation techniques include the multi-effect distillation (MED), multi-stage flash (MSF), vacuum distillation (VD) and vapour compression distillation (VCD)

2.2.1 Multi-effect distillation (MED)

This process uses different chambers to act as heat exchangers and these chambers are called effects. In this technique, the feed water is preheated to boil before being fed to the various vessels.

In each effect, the heated saline feed water is sprayed on the surface of the tube which is the evaporator surface and then the tube is heated by steam which also allows the steam inside

the tube to condense. A portion of the water gets evaporated and then the steam enters the tube of the next effect. Vapour produced in the first effect is used to heat the evaporator in the next effect and the cycle of evaporation and condensation continues. In the last effect, the vapour from it is condensed in the final condenser and cooled by the incoming feed water (Khan et al., 2021). MED produces high-purity distillate, consumes low electricity (<1.0 $kWhm^{-3}$) and is operated at low temperatures (<70°C) (Lange, 2013).

2.2.2 Multi-stage flash (MSF)

MSF is a thermal desalination technology used to distill saline water. It is composed of a series of stages and in each stage, the seawater is preheated by a condensing steam. The heated saline water is made to pass through a chamber with lowered ambient pressure which forces it to almost flash into steam while the remaining saline water passes through the next stage of flashing (Shatilla, 2020).

MSF is a process of desalination that occurs by flashing some quantity of polluted water into multiple stages and the pressure and saturation temperature of every stage are fewer than those of the previous unit stage (Essa et al., 2022). MSF requires minimum pretreatment and has a low fouling potential. However, the factors that affect the efficacy of MSF units include the number of stages, skilled operators, and maintenance cost (Shatilla, 2020).

2.2.3 Vacuum distillation

This technique is used to desalinate seawater and brackish water. The process of vacuum distillation works by decreasing the pressure of the saline water which then causes the water to boil at a lower temperature (lowered boiling point). When this happens, the saline water gets evaporated and the vapour is condensed and collected as freshwater (Essa et al., 2022).

2.2.4 Vapour compression distillation (VCD)

In this process of distillation, seawater or brackish water is evaporated and converted to high purity water for domestic and industrial purposes by the application of heat delivered by compressed vapour. The basic principle of VCD is the reduction of the boiling temperature by the reduction of the ambient pressure. There are two methods used to carry out VCD operation and they are mechanical vapour compression MVC (usually electrically driven) and thermal vapour compression TVC (uses a steam jet ejector). In MVC, the compressor compresses the vapour and increases its enthalpy. The seawater feed cools down the distillate

in the tube side of the evaporator and also cools the brine. After cooling, the brine is rejected to the outside of the system. In TVC, some amount of vapour produced in the vessel is diverted and recompressed by a steam ejector. A mixing chamber mixes both the vapour and steam and they are then compressed through a diffuser and enter the evaporator to be used again as heating steam. Then the rest of the vapour is sent to a condenser to preheat the seawater feed (Shatilla, 2020).

2.2.5 Humidification-dehumidification (HDH)

HDH is a thermal water desalination technique that is based on evaporation and condensation of the generated humid air mostly at ambient pressure. The working principle of HDH depends on the fact that some amount of water vapour is contained in the air and the amount of vapour carried is proportional to the temperature of the air. For example, when the temperature of the air is raised from 30 $^{\circ}$C to 80 $^{\circ}$C it could cause 0.5 kg of vapour to be carried by 1 kg of dry air and around 670 kcal (Morris and Hanbury, 1991).

When airflow is in contact with saline water, some quantity of vapour is extracted by the air at the expense of the heat of salt water (providing cooling). The distilled water is recuperated by maintaining humid air at contact with cooling surface, and this leads to the condensation of a part of the vapour mixed with the air. Some of the advantages of HDH includes having simple equipments, moderate cost of asset and operation, flexible scale and available low-grade energy (Kabeel et al., 2013).

2.3 Solar Still (SS)

A solar distiller also known as a solar still is a technique used for water desalination and purification, and is the main subject of the present study. The basic principle of the solar distiller is derived from the hydrological cycle which is the continuous circulation of water in the atmosphere through the aid of evaporation and condensation. The solar still is a basin constructed with a transparent glass cover that is inclined at an angle for the purpose of water collection. The basin contains the sea or brackish water or generally the contaminated water which gets heated up by the sun that passes through the transparent glass cover. The heated water evaporates and condenses on the inner surface of the glass cover. Due to the inclination of the glass cover, the condensed water droplets run down and are collected in a trough or gutter pipe which is connected to a PVC pipe that allows the water to flow out of the still into a clean plastic container.

The condensed water is collected as freshwater leaving the concentrated salty water behind in the basin. Figure 2.3 shows a schematic diagram of a solar still.

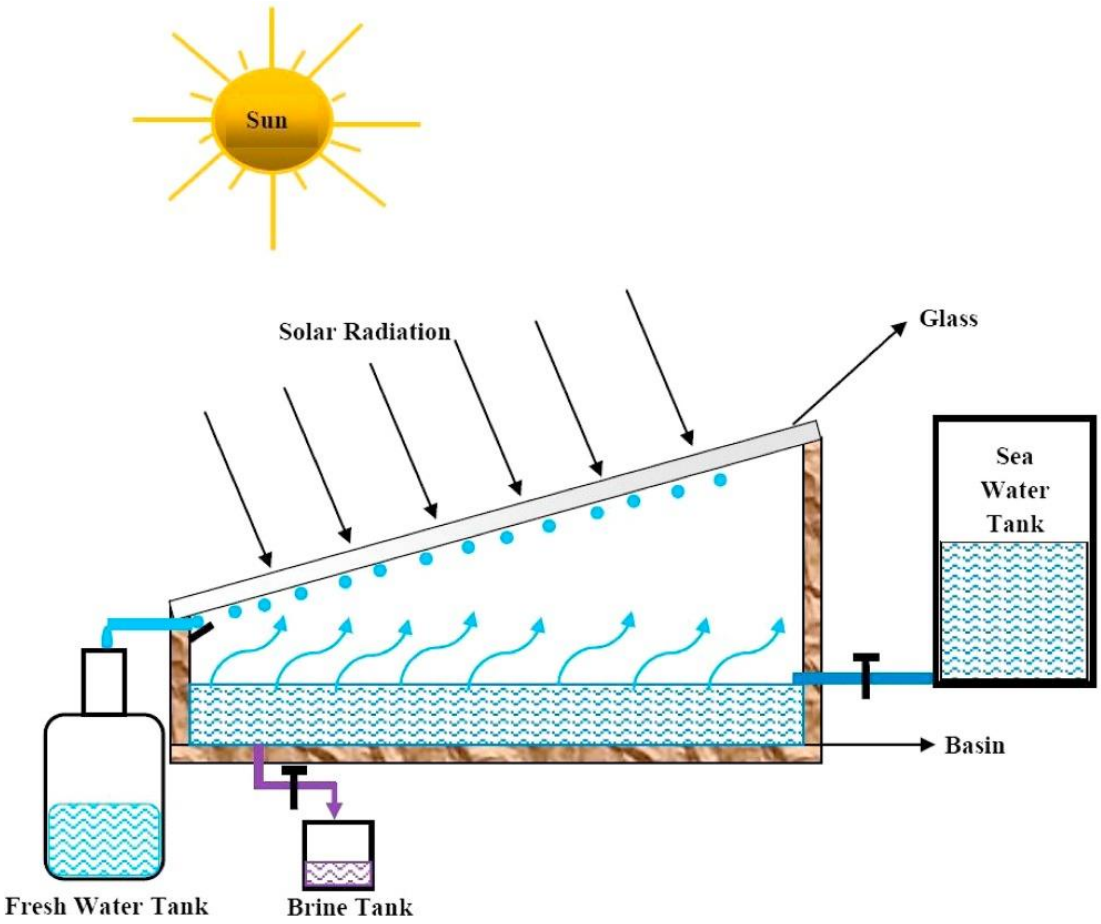

Figure 2.3: A typical solar still system (Sharon & Reddy, 2015).

The major advantages of the solar still are the materials are cheap, the ease of construction and it is ideal for family-size applications, especially in rural areas, but the main disadvantage is its inability to produce large quantity of freshwater and as a result of this, there are various factors to be considered while constructing the solar still to improve the performance and productivity of the still. In the following paragraphs categories of solar still, its advantages and disadvantages, its efficiency maximisation, and comparison to reverse osmosis are presented.

2.3.1 Categories of Solar Still

Solar stills are categorised into active and passive solar stills. Both receive energy from the sun which raises the temperature of the basin water and causes evaporation and condensation. An active solar still uses the energy from the sun combined with a solar thermal collector to raise the temperature of the salt water. A passive solar still utilizes only the energy from the sun to raise the temperature of the water. Active solar stills have higher productivity and efficiency than passive solar stills (Tiwari and Sahota, 2017) but have a more complex design, requiring more resources like electricity. A passive solar still remains a sustainable and cost-effective method as it requires no power supply, skill, professionalism to operate and would be very beneficial to rural and off-grid areas.

2.3.2 Solar Still Advantages over Distillation and Reverse Osmosis Techniques

Solar still has some comparative advantages over distillation and reverse osmosis techniques. Low-cost materials are used in the construction of a solar still; water treatment equipment, complex water pumping machine and logistics transportation are not required; and it can be used in regions with little or no development and infrastructures (Delyannis and Belessiotis, 2004).

2.3.3 Factors affecting the efficiency of a Solar Still

The performance of a solar still is affected by different factors or parameters which include meteorological factors, design factors, and operational factors (Essa et al., 2022). These factors are illustrated in Figure. 2.4.

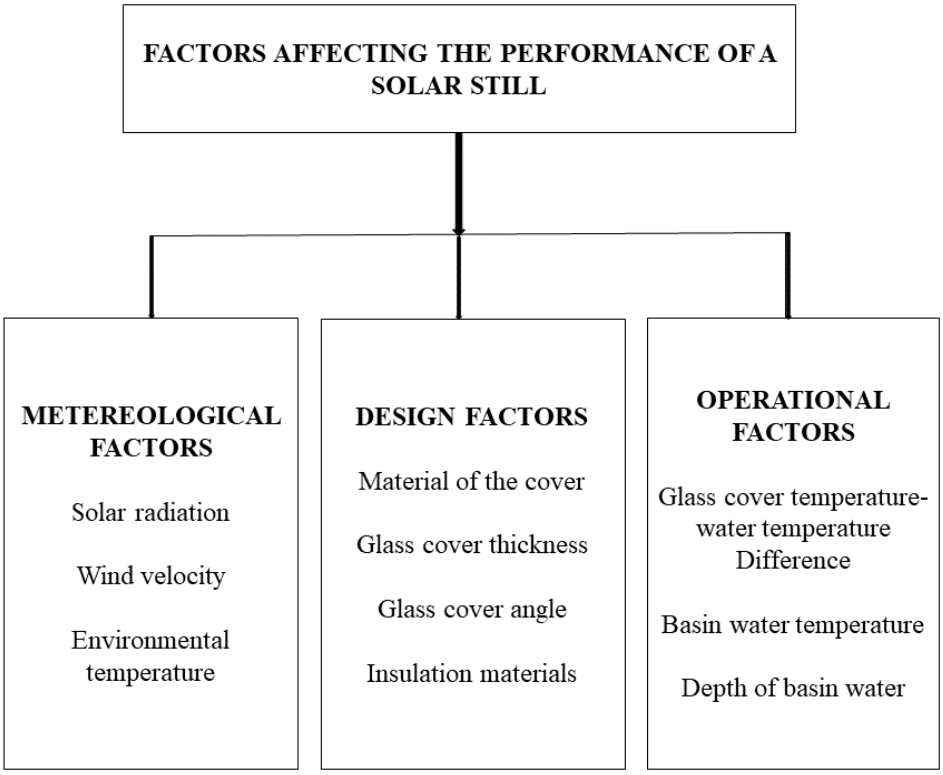

Figure 2.4: Factors that affect the performance of a solar still. Adapted from (Essa et al., 2022).

2.3.3.1 Meteorological Factors

The meteorological factors include the intensity of solar radiation, wind velocity and environmental temperature, known as climatic factors, which have huge effect on the performance of a solar still but cannot be controlled. This factor is so important that it also affects the water-glass temperature difference as well as the convective and evaporative heat transfer coefficients (Essa et al., 2022). A description of solar radiation, wind velocity and environmental temperature are briefly presented in the following paragraphs.

2.3.3.1.1 Solar radiation

Solar radiation is the energy emitted by the Sun through electromagnetic waves. The intensity of solar radiation greatly affects the performance of the solar still and this varies with the location, time, and weather of a particular location. The amount of radiation that gets to a surface is dependent on the angle of the sun above the horizon, the length of time at which the surface is exposed to the sun, and atmospheric conditions.

The efficiency and productivity of the solar still are increased by the increase in intensity of solar radiation and this explains why solar stills achieve their highest efficiency between 10 am and 2 pm as during that time, the temperature of the water increases which also causes faster evaporation (Narayanan et al., 2020). Okeke et al., (1990) also explained that solar radiation increases the convective heat transfer coefficient by heating the basin water which then results in faster evaporation, hence, an increased efficiency.

2.3.3.1.2 Wind velocity

Wind velocity affects the temperature of the glass cover because the higher wind velocity leads to an increase in the convective heat transfer from the cover to the atmosphere and as a result, there is an increased evaporation, increased condensation rate, and then an increased performance of the solar still (Sharshir et al., 2016). The speed of wind flowing over the glass plate has a significant effect on the performance of the solar still because as the wind speed increases, the convective heat transfer from the top of the glass surface reduces the temperature of the glass surface and as a result of this, more distillate condenses on the inner surface of the glass cover, thereby increasing the productivity of the solar still (Narayanan et al., 2020). An experiment was performed on an active and passive solar still and the influence of different air speeds was observed, and then confirmed that increasing the ambient air speed enhances the performance of a solar still (El-Sebaii, 2000).

2.3.3.1.3 Environmental temperature

Environmental temperature refers to the average temperature of the surroundings and is also called ambient temperature. It is dependent on the location, time of the day, and other climatic factors. Different researchers gave different opinions on the effect of environmental factors on the productivity of a solar still. Al-Hinai et al., (2002) reported that raising the environmental temperature by 10°C (23-33°C) improved the output by 8.2%. Raising the temperature of the air in the surrounding plays a crucial role in the performance of the solar still by increasing the daily air temperature from 34.51°C – 38.15°C thereby getting a yield of 3200 mL/m^2 from the initial 1750 mL/m^2 (Alheefi, 2019).

2.3.3.2 Design Factors

These are factors that can be controlled and varied in order to achieve greater use and productivity of the solar still. These include the material of the cover, thickness of the glass cover, glass cover angle, insulation material.

2.3.3.2.1 Material of the cover

The material used in constructing the cover of the solar still is crucial since it is only through the cover that the solar radiation would get to the basin water. The amount of solar radiation that gets into the basin water is dependent on the thermal conductivity of the cover of the solar still. Different materials such as plastic and copper possess different thermal conductivities and researchers have studied these various materials (Dimri et al., 2008).

2.3.3.2.2 The thickness of the glass cover

The key role of the glass in the solar still is to allow the penetration of solar radiation with high thermal energy and block the longer wavelengths. With this, the distiller captures a maximum amount of solar radiation and does not radiate back the solar intensity (Essa et al., 2022).

Ghoneyem and Ileri (1997) constructed and tested four single-effect basin-type solar stills, three of the stills had the cover made of glass of different thicknesses (3, 5, 6 mm) while the fourth cover was made of plastic. It was observed that the still made with 3 mm glass cover had the highest production rate of 15.5%.

2.3.3.2.3 Glass cover angle

This is also known as the slope or inclination of the glass cover. The angle of the glass cover should be made such that it minimizes the reflection of the sun from the cover and also in a way that the droplets of the condensed water trickle down to the collector and do not fall back to the basin water (Narayanan et al., 2020). Different groups experimented using different angles and it has been observed that different angles of the glass cover give different yields of the solar still.

Singh and Tiwari (2004) studied the annual yield of active and passive solar stills at different locations having different climatic conditions and observed that maximum yield is achieved when the slope of the glass cover is the same as the latitude of the place. Akash et al., (2000) reported on five different angles of the glass cover (15°, 25°, 35°, 45° and 55°) in Jordan (latitude $30'58^{\circ}$), and it was observed that the highest yield occurred at 35°. (Akash et al., 2000) also got a maximum yield in the month of May using an inclination angle of 35°.

Aybar et al., (2005) suggested that making an inclination of 30° increases the amount of solar radiation reaching the surface aperture more frequently during the day and also allows the

water to run down easily. In 2009, Khalifa and Hamood found that changing the slope of the glass cover could alter the productivity of the solar still by almost 63%. This was further confirmed by Narayanan et al., (2020) who were of the view that if the slope is made too low, there will be a reduction of the speed of the droplets flowing on the inner surface of the glass and this would tend to increase the rate at which the droplets fall into the basin instead of the condensate collector. If the slope is increased or made too high, there will be an increase in the surface area of the cover which is also an increase in thermal losses.

2.3.3.2.4 Insulation materials

Insulation materials are used to prevent heat transfer. The idea is that only the upper surface of the water evaporates and thus the bulk water need not be heated, and should be insulated from the sun's heat as much as possible. In choosing an insulation material, the thermal conductivity of the material chosen should be extremely low to prevent the transfer of heat from the basin to the external environment. This is in line with Cöuras Ford et al., (2008) (Cöuras Ford et al., 2008) observed the effect of properties of various insulation material on the performance of the solar still and found that the composite based on gypsum and expanded polystyrene (EPS) proved to be good thermal insulation for the distiller. Khalifa and Hamood (2009) demonstrated that the increase in insulation thickness increased the production of the solar still by up to 80% as the productivity increased from 1.81 L/m^2 day for a still without insulation to 3.28 L/m^2 for a still with insulation thickness of 60 mm to 100 mm (Khalifa & Hamood, 2009). Hashim et al., (2009) invented five different symmetric double slope single basin solar stills. One without insulation and the other four with different insulation materials such as 5 mm thick air gap, plywood, hay-plywood glasswool-plywood. The productivity of the solar stills was observed to increase by 74%, 82%, 126% and 130% respectively (Hashim et al., 2009).

2.3.3.3 Operational Factors

Operational factors refer to practical conditions necessary for efficient and productive solar still function. These factors include the glass temperature-water temperature difference, depth of basin water, and basin water temperature.

2.3.3.3.1 Glass cover temperature - water temperature difference

The temperature difference between the glass cover temperature and the basin water temperature is the most important regulating factor in optimising yield from a solar still (Sarkar et al., 2022). The temperature difference between the glass cover and basin water can be done in the following ways: increasing the temperature of the basin water, decreasing the temperature of the glass cover, or combining both strategies together. The increased temperature of the water will increase the evaporation rate while the reduced temperature of the glass cover will increase the condensation rate and this will lead to more production of the solar still (Sarkar et al., 2022). Sarkar et al., 2022 stated that cooling the glass with water not only improves the production of the still but also cleans the dust particles that settle on the glass cover which could reduce the amount of solar radiation reaching the water in the basin. In order to obtain the water-glass temperature difference, the glass cover is cooled by water film which also cleanses the glass from dirt that can diminish the efficiency of the still (Omara et al., 2017).

These scholars confirmed earlier findings by Tiwari and Rao, (1984) that flowing water on the glass cover at a uniform velocity nearly doubles the daily distillate output of the solar still.

2.3.3.3.2 Basin water temperature

The basin water is heated up by the solar radiation from the sun which passes through the glass cover and permeates the water. Raising the temperature of the water contained in the basin increases the rate of evaporation and as well increases the productivity of the solar still.

Rubio et al., (2000) evaluated the distillate yield for a double slope laboratory still under controlled conditions for basin water and the productivity of 0.8 L/m^2/h was obtained when the brine/basin water temperature was 70°, whereas the productivity was reduced to reach a value of 0.10 L/m^2/h when the brine temperature became 30°C.

2.3.3.3.3 Depth of basin water

It has been established that the lower the depth of the basin water, the higher the rate of the convective heat transfer and the higher the productivity of freshwater (Tiwari & Tiwari, 2007). Elango and Murugavel (2015) experimented on double slope distiller and single slope distiller under various water depths of 1, 2, 3, 4 and 5 cm and observed that the optimum

basin water depth is 1 cm for both single and double basin slope solar stills (Elango & Murugavel, 2015). Dimri et al., (2008) proved that the yield of the solar still decreases with increase of water mass from 20 to 150 kg and attributed the decrease to be a result of higher specific heat capacity of water by the mass of water increased (Dimri et al., 2008).

2.4 Interfacial Evaporation

This is a process whereby there is localised heating at the surface of the water body which results in the formation of water vapour. This phenomenon occurs at the liquid/air interface and is a promising alternative to bulk heating-based evaporation that allows the entire water body to get heated as evaporation takes place. Solar-driven interfacial evaporation has been proven to achieve an efficiency of ~90% because of its ability to reduce thermal losses due to the bulk-heating (Tao et al., 2018).

This state-of-the-art approach has been a game-changing solution to water shortage being that water molecules will continue to escape so long as the energy from the sun remains constant until the vapour is saturated or the water is consumed completely, thereby generating clean water in the process and at the same time, increasing the yield of the water being produced.

A solar interfacial evaporation system is made up of three key components as shown in Figure 2.5 which are photothermal materials, heat management and water supply and each of these components increases the performance and efficiency of the solar still. The photothermal material contains an absorber, a wicking structure and an insulator. These materials can be made with materials of different kinds including biocompatible materials and in order to achieve long-term stability, the materials must possess excellent durability and salt resistance (Yan et al., 2022). Heat management is simply a way to reduce heat losses from heated water. An insulator is placed between the evaporation structure or material and the bulk water in order to prevent downward heat loss by conduction thereby allowing only the surface of the water to remain heated up while the bulk water is left cold. Water supply is of huge importance for evaporation to occur and a sufficient supply of water is needed (Zhang et al., 2020).

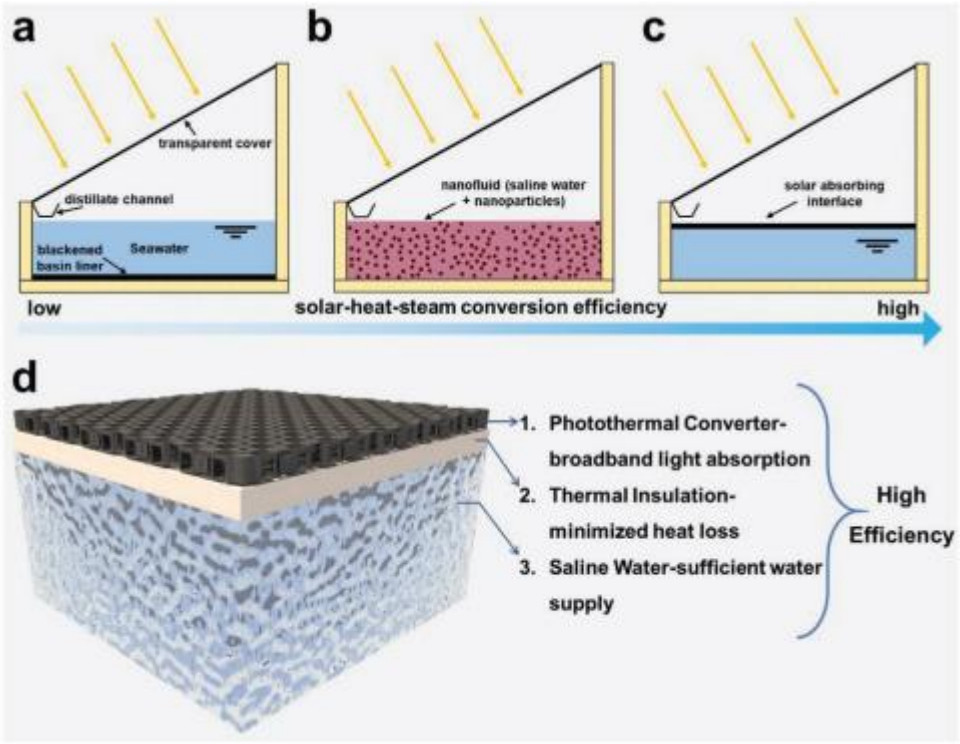

Figure 2.5: (a,b,c) Different forms of solar heating with the absorber placed at different points or locations in the water. (d) Three components of solar interfacial evaporation (Zhang et al., 2020).

2.4.1 Evaporation structure

For evaporation to occur, sufficient water has to be supplied to the absorber at the surface. Underneath the solar absorber is a structure that draws water from the system to the solar absorber. This can be seen in figure 2.6 where the solar absorber is heated directly by the sun. It could also be seen that the insulator having a low thermal conductivity prevents the water below from getting heated directly by the sun, or indirectly by conduction and convection. Capillary action enables the structure to wick up water and mechanically and autonymously pump it to the surface where heating occurs. Some of the factors to be considered when choosing an evaporation structure are the porosity and the surface wettability of the material. Different materials such as cotton (Ni et al., 2016), cellulose fabric (Ni et al., 2018) have been fabricated and used as an evaporation structure.

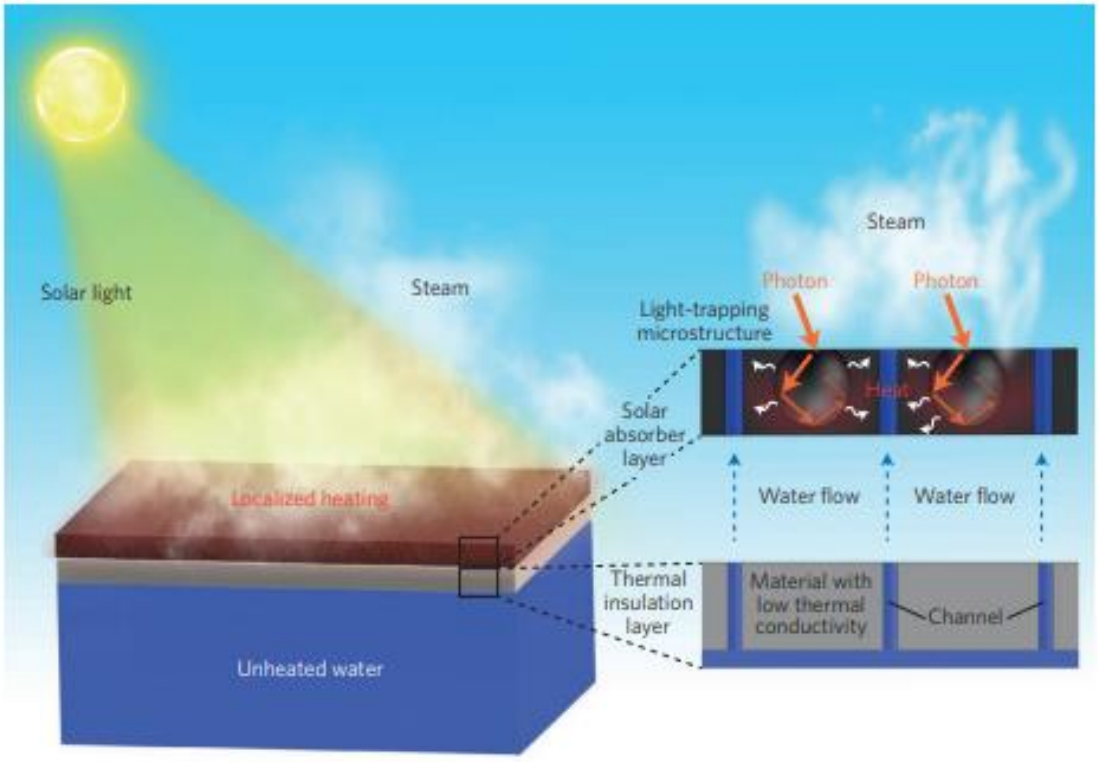

Figure 2.6: Structure and operation of an evaporation structure floating at the water-air interface (Shang & Deng, 2016)

2.4.2 Solar absorber

A solar absorber is a material that can absorb the energy from the sun or solar radiation, efficiently convert it to heat, and then deliver the heat to a system. A spectrally-selective absorber has strong solar absorptance (0.25–2.5 μ m) and low infrared emittance. The emittance of an ideal spectrally-selective absorber is 1 at short wavelengths and 0 at long wavelengths (Cao et al., 2014). Solar absorbers with broadband light absorption tend to achieve higher efficiencies, therefore, broadband light absorption in the range of 300 to 2500 nm is desired for a high performance (Zhang et al., 2020).

Various forms of solar heating with the absorber placed at different points or locations in the water have been experimented on as illustrated on Figure 2.5 (a,b,c). These forms of solar heating include bottom heating, bulk heating, and surface heating. Bottom heating is where an absorber plate which could be a metal sheet is painted black and placed just below the water to absorb the solar radiation. It gets heated up and heats up the bulk water as well, and then increases the evaporation efficiency (Arunkumar et al., 2019). The efficiency of this

design is quite low as the heat generated is lost to the bulk water and also to the surrounding through conduction, convection and radiation.

In bulk heating, also known as volumetric heating, solar absorbers are dispersed into the bulk water converting the incident solar photons into thermal energy to heat the entire liquid (Tao et al., 2018). When the nanoparticle solar absorbers are dispersed in the liquid, vapour is generated around the particles as the light illuminates the solution. The vapour-enveloped nanoparticle then travels to the air-water interface and releases the vapour into the air without raising the temperature of the liquid (Liu & Song, 2018).

Surface heating, also known as interfacial heating, involves heating up the liquid at the liquid-air interface. This has become the state-of-the-art approach in water desalination as scientists now achieve evaporation efficiencies greater than 90%. So far, the most prominent feature of solar interfacial evaporation is placing the solar absorber between the saline liquid and air. This design minimises heat lost to the bulk water and provides more surface area for vapour release.

To achieve high efficiencies, different materials have been explored in the fabrication of solar absorbers, and further research is ongoing. Solar absorbers could be made of hydrophilic or hydrophobic materials. Hydrophilic materials possess improved water transport structures while hydrophobic solar absorbers possess self-healing structures that are coupled with hydrophilic wicks that draw water to its surface (Zhang et al., 2020). The hydrophobic structures can prevent salt formation on the surface because the salt ions are deposited and dissolved in the hydrophilic layer because of a continuous supply of water (Xu et al., 2018). The hydrophobic materials also help to float the solar absorbers as can be seen in hollow carbon spheres (Zeng et al., 2011). In as much as the hydrophobic materials can float and self-clean to get rid of contaminants and salts clogging their pores, their evaporation rate is reduced as there is a restriction of heat and mass transfer (Tao et al., 2018).

There are two categories of solar absorbers, namely carbon-based (which includes graphite, carbon nanotubes, graphene, activated charcoal, etc.) and plasmonic-based (which includes gold, silver, copper and their compounds) (Tao et al., 2018). In carbon-based materials, solar absorption involves the excitation and relaxation of electrons and they are suitable for broadband solar absorption (Kuzmenko et al., 2008). Its low cost, excellent light-to-heat conversion properties and reusability are the reasons why the carbon-based absorbers are widely used (Shi et al., 2017).

Generally, carbon materials are prepared from natural materials by carbonization. Some of the natural materials include sugarcane (Zhang et al., 2022), bamboo (Li et al., 2019), natural green flora (Arunkumar et al., 2022), loofah (Ren et al., 2021), corn stalks (Sun et al., 2020) etc. These materials are also known as plant-based photothermal materials. Among all these, reduced graphene oxide (Fan et al., 2020), graphene oxide (Guo et al., 2017), and carbon fibers (Ma et al., 2020) are good materials because of their low cost and high absorptance.

An example of a plasmonic nanoparticle is gold (Au). Unlike carbon materials, it only absorbs a narrow band of light around its resonance peak. In order to cover a wider portion of the solar spectrum, plasmonic nanoparticles can be modified to cover a wider range of wavelengths by size, shape and structure adjustment and orientational arrangement (Zhang et al., 2020). To do this, plasmonic nanoparticles are assembled into porous films wherein the Au nanoparticles are closely packed. Their individual localized surface plasmon resonance modes overlap and hybridize with each other and this leads to broadband absorption (Tao et al., 2018).

2.4.3 Wicking structure

Wicking is the ability of a liquid to travel through a material by capillary action. It is a result of the intermolecular forces of adhesion (between the material and the liquid) and cohesion (inside the liquid). The ability of a liquid to maintain contact with another surface is known as wetting. This occurs when the liquid molecules have greater attraction to the molecules of the solid material (liquid-solid interface) than to each other (liquid-liquid interface). When this happens, it means that the adhesive force is greater than the cohesive force. The phenomenon of wetting leads to wicking and this can only occur in porous materials.

If the molecules of the liquid are more attached than to the molecules of the solid, then it means that the cohesive forces are greater than the adhesive forces and this leads to the liquid not spreading across the surface of the material.

Water supply is of utmost importance in the management of heat and the rate of evaporation (Yan et al., 2022). Researchers have conducted various experiments using different wicking materials and concluded that solar stills with wicking structures are more efficient than those without them. Murugavel et al., (2008) incorporated cotton and jute as wick materials. Ashish et al., (2022) assert using PVA, cotton cloth, and air laid paper (ALP) as wicking structures and concluded that PVA was the most effective among the three materials examined because

of its mesh-like structure with open pores. The evaporative efficiency of PVA, cotton cloth and ALP were 78%, 38% and 24% respectively.

2.4.4 Water pathways

These are ways in which water is transported from the bulk water to the solar absorber. This design was put forward in a bid to reduce or eliminate heat loss from the solar absorber to the bulk water and is a crucial factor for obtaining continuous and efficient water transport (Chen et al., 2019). The water pathway designs can be classified as 3D, 2D, and 1D pathways. In 3D pathways, the solar absorber is in direct contact with the bulk water which is transported through porous substrates to the surface of the solar absorber. The disadvantage of this design is that under wet conditions, there is an increased thermal conductivity which results in heat loss to the bulk water through conduction (Chen et al., 2019; Wang et al., 2019). In order to minimize the contact with water, a 2D pathway design was proposed. This design enables an efficient supply of water and suppresses heat loss. An insulator is used here, alongside a wicking structure that conveys water to the solar absorber. (Li et al., 2016) wrapped the thermal insulator with a thin layer of hydrophilic cellulose which provided a 2D pathway for water wicked up to the graphene oxide (GO) film absorber by capillary effect. This design reduces heat lost to the bulk water by conduction by reducing the volume of the water path. In a 1D water pathway, heat loss due to conduction, convection and radiation is minimized. This is achieved by pumping water upward to the solar absorber using a 1D artificial stem (wicking materials). Wang et al., (2018) designed a 1D pathway structure using a 3D photothermal cone structure. It was shown that lowering the dimension of water supply, the solar evaporator increases the evaporation area as the contact area decreases thereby leading to suppressed heat loss and high solar conversion efficiency.

2.4.5 Insulation material

One of the challenges of a solar still is heat loss. Different approaches have been used to reduce heat loss in the solar still. For interfacial evaporation, an insulation material is used to reduce the heat lost to the bulk water via downward conduction. One good example of an insulation material is polystyrene. When expanded into foam it is called expanded polystyrene, also known as Styrofoam, it fits perfectly as an insulator because it has a high thermal resistance.

Among the reports who experimented using polystyrene as a thermal insulator is (Ni et al., 2016) who drilled a channel through a polystyrene foam and then threaded through the hole with hydrophilic cotton which used capillary action to deliver water to the absorber. The polystyrene foam served as an insulation material by preventing heat from getting to the bulk water by limiting the thermal conduction and radiation to the cool water underneath, and at the same time, it floated the entire structure on the water body. Li et al., (2016) also used polystyrene as insulation material. They wrapped it with hydrophilic cellulose whose capillary wicking effect drew up and pumped water to the heating surface.

2.4.6 Polystyrene

Polystyrene (PS) is a hard and stiff synthetic polymer produced by the polymerization of styrene. Due to its inert, cost-effective and long-lasting properties, it is the most widely used plastic in several industries in the production of automotive, home appliances, packaging materials, cartons, disposable plates, cups, trays etc. They are also widely used as insulation for building walls, roofs, refrigerators, and industrial cold storage facilities. Polystyrene is recyclable and also used in the medical industries because of its low cost, low density, clarity, dimensional adaptability to radiation sterilization (Wagner 2020).

2.4.7 Chemistry of polystyrene

The chemical formular of polystyrene is $(C_8H_8)_n$, and its chemical structure is shown in figure 2.7. It has a molecular weight of 104.1g/mol and a density of 1.04 g/cm^3. PS is non-polar because it contains only carbon-hydrogen bonds, hence it is insoluble in water but soluble in organic solvents such as toluene, acetone etc. It has a melting point of approximately 240°C.

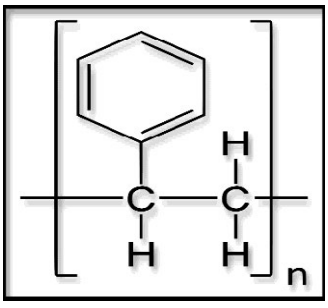

Figure 2.7: The chemical structure of polystyrene

Like other organic compounds, polystyrene undergoes combustion to give carbon dioxide, water vapour and other by-products. Pyrolysis is the process by which polystyrene is depolymerized into its monomer styrene. In this process, large amount of heat and a high pressure is used to break the chemical bonds between each of the styrene compounds.

Polystyrene is produced in different forms but the most common and primary types are expanded polystyrene (EPS) and extruded polystyrene. Expanded polystyrene is a lightweight closed-cell plastic foam with a density ranging from 11 to 32 kg/m^3. It consists of small hollow spherical balls that are expanded by molding. It is composed of air and has excellent insulation properties.

In the production of extruded polystyrene, PS granules are fed into an extruder where they are melted and mixed, and then a blowing agent is injected to allow the expansion of the plastic. Under controlled heat and pressure, the plastic mixture is then forced or extruded through a die. The extruded foam then cools and expands into its final shape. Extruded Polystyrene foams have tightly packed closed-cell structure that make them strong and rigid.

2.4.8 Tyre dust as a black pigment used as solar absorber

Pigments are organic or inorganic finely ground particles naturally or synthetically made that impart colour when added to paints or formulations. They are known to be insoluble in the medium in which they are dispersed and make up a large percentage of the medium.

2.5 Efficiency of a solar still

The efficiency of solar-vapor conversion, Ƞ is defined as:

$$\eta = \frac{\dot{m} h_{fg}}{q_{solar} A_{evap}} \quad \text{.....(1)}$$

where ṁ is the mass flux or evaporation rate in kg m^{-2} h^{-1}, h_{fg} is the latent heat of vaporization of water which is the total enthalpy demanded to turn liquid water into vapour, q_{solar} is the incoming solar flux and A_{evap} is the area of the absorber surface exposed to the incoming solar flux.

The latent heat should be determined with the surface temperature of solar evaporators since it is not constant. The latent heat of water phase-change enthalpy on a 40° solar absorber is

2406 kJ kg^{-1}, and it would be 2256 kJ kg^{-1} on a 100° surface (Zhang et al., 2020). The efficiencies and evaporation rates of some photothermal materials used by different authors are listed in table 2.1 below.

Table 2.1: Efficiencies and evaporation rates attained using different materials as photothermal materials in solar interfacial evaporation.

Photothermal materials used	**Evaporation rates and efficiencies obtained.**
Graphene oxide	89.2% (Guo et al., 2017).
Cellulose based fabric and expanded polystyrene	2.5 L $m^{-2}day^{-1}$ (Ni et al., 2018).
Hierarchical nanostructured gels (HNGs)	3.2 kg m^{-2} h^{-1} (Zhao et al., 2018).
Carbon fiber	1.49 kg m^{-2} h^{-1} (90%) (Chen et al., 2019).
Reduced graphene oxide	4.54 kg m^{-2} h^{-1} (97%) (Ma et al., 2020).
Thermally localized multistage solar still	5.78 L m^{-2} h^{-1} (Xu et al., 2020).
Carbon Nanotubes	1.372 kg m^{-2} day^{-1} (86.1%) (Liang et al., 2021).
Lignin hydrogel-based	2.25 kg m^{-2} h^{-1} (Jiang et al., 2022).
PVA/activated carbon sponge	4.47 kg m^{-2} h^{-1} (Liang et al., 2022).

2.6 Water Hardness

This is the total calcium and magnesium ion concentrations contained in a water sample, and is classified as (a) soft water – which contains less than 17 parts per million (ppm) Ca and Mg ions; slightly hard water – containing between 17 to 60 ppm Ca and Mg ions; moderately hard water – containing between 60 to 120 ppm Ca and Mg ions, and hard water – containing between 120 to 180 ppm of Ca and Mg ions.

Water hardness is expressed as the mass in milligrams per litre of calcium carbonate water containing the same number of dipositive (2+) ions. It is also a measure of the concentration of divalent metal ions such as calcium (Ca^{2+}) and magnesium (Mg^{2+}) per volume of water. Water hardness can be temporary or permanent. It is temporary when there is the presence of calcium bicarbonate and magnesium bicarbonate and also hydroxides of calcium and magnesium and can be eliminated by boiling. On boiling, the soluble salts of $Mg(HCO_3)_2$ are converted to $Mg(OH)_2$, which is insoluble, and hence gets precipitated and is removed.

$Ca(HCO_3)_{2\ (aq)} \rightarrow CaCO_{3(s)} + H_2O_{\ (l)} + CO_{2\ (g)}$ ----------(2)

$Mg(HCO_3)_{2\ (aq)} \rightarrow MgCO_{3(s)} + H_2O_{\ (l)} + CO_{2\ (g)}$ ----------(3)

Equation 2 and 3 represents the chemical equations of temporary hardness.

Water is said to be permanently hard when it contains salts of calcium and magnesium in the form of sulphates, chlorides, and nitrates and cannot be eliminated by boiling. Permanent hardness can be removed by:

- Distillation
- Ion exchange
- Use of calcium hydroxide (lime) and sodium carbonate (soda ash)
- Chelation
- Reverse osmosis.

2.6.1 Effects of water hardness

The following are caused by hard water:

- Scale build-up and deposit on pipes, walls, containers and tiles
- Stains water fixtures
- Reduces the washing and foaming effect of soap, hence it wastes soap.

References

Akash, B.A., Mohsen, M.S., Nayfeh, W. (2000). Experimental study of the basin type solar still under local climate condition. *Energy Conversion and Management*, *41*(9), 883–890.

Alheefi, T. (2019). *Experimental and analytical study of water production of solar still*. Brunel University London.

Alnaimat, F. (2011). *Transient analysis of solar diffusion driven desalination*. University of Florida.

Alnaimat, F., Klausner, J., Matthew, B. (2018). Solar desalination. In *Desalination and water treatment* (pp. 128–150). intechopen. https://doi.org/http:\\dx.doi.org\10.5772\intechopen.76981

Arunkumar, T., Lim, H, W., Denkenberger, D., Lee, S, J. (2022). A review on carbonized natural green flora for solar desalination. *Renewable and Sustainable Energy Reviews*, *158(C)*, 112121.

Arunkumar, T., Raj, K., Dsilva Winfred Rufuss, D., Denkenberger, D., Tingting, G., Xuan, L., & Velraj, R. (2019). A review of efficient high productivity solar stills. *Renewable and Sustainable Energy Reviews*, *101*(August 2018), 197–220. https://doi.org/10.1016/j.rser.2018.11.013

Bajraktari, N., Madsen, H. T., Gruber, M. F., Truelsen, S., Jensen, E. L., Jensen, H., & Hélix-Nielsen, C. (2016). Separation of peptides with forward osmosis biomimetic membranes. *Membranes*, *6*(4), 1–12. https://doi.org/10.3390/membranes6040046

Bardhan, A., Akhtar, A., Subbiah, S. (2022). Microfiltration and ultrafiltration membrane technologies. *Advancement in Polymer-Based Membranes for Water Remediation*, 3–42. https://doi.org/https://doi.org/10.1016/B978-0-323-88514-0.00001-2

Cao, F., McEnaney, K., Chen, G., & Ren, Z. (2014). A review of cermet-based spectrally selective solar absorbers. *Energy and Environmental Science*, *7*(5), 1615–1627. https://doi.org/10.1039/c3ee43825b

Charcosset, C. (2012). *Membrane Processes In Biotechnology and Pharmaceutics*. Elsevier

B.V. https://doi.org/https://doi.org/10.1016/C2011-0-04261-8

Chen, L., Xia, M., Du, J., Luo, X., Zhang, L., Li, A. (2019). Superhydrophillic and oleophobic porous architectures based on basalt fibers as oil-repellant photothermal materials for solar steam generation. *Chemistry-Sustainaibility-Energy-Materials*, *13*(3), 493–500.

Chen, C., Kuang, Y., & Hu, L. (2019). Challenges and Opportunities for Solar Evaporation. *Joule*, *3*(3), 683–718. https://doi.org/10.1016/j.joule.2018.12.023

Cöuras Ford, E. T. L., Ribeiro, F. A., Lima, R. V., & Souza, E. M. (2008). Solar Distiller in a Pyramidal Covering and Isolation With Composite Material. *Revista de Engenharia Térmica*, *7*(1), 37. https://doi.org/10.5380/reterm.v7i1.61739

Delyannis, E., Belessiotis, V. (2004). Solar Water Desalination. In *Encyclopedia of Energy* (pp. 685–694). Elsevier. https://doi.org/https://doi.org/10.1016/B0-12-176480-X/00321-1.

Dimri, V., Sarkar, B., Singh, U., & Tiwari, G. N. (2008). Effect of condensing cover material on yield of an active solar still: an experimental validation. *Desalination*, *227*(1–3), 178–189. https://doi.org/10.1016/j.desal.2007.06.024

El-Sebaii, A. A. (2000). Effect of wind speed on some designs of solar stills. *Energy Conversion and Management*, *41*(6), 523–538. https://doi.org/10.1016/S0196-8904(99)00119-3

Elango, T., & Kalidasa Murugavel, K. (2015). The effect of the water depth on the productivity for single and double basin double slope glass solar stills. *Desalination*, *359*(December), 82–91. https://doi.org/10.1016/j.desal.2014.12.036

Fan, X., Lv, B., Xu, Y., Huang, H., Yang, Y., Wang, Y., Xiao, J., Song, C. (2020). Electrospun reduced graphene oxide/polyacrylonitrile membrane for high-performance solar evaporation. *Solar Energy*, *209*, 325–333. https://doi.org/https://doi.org/10.1016/j.solener.2020.09.013

Garud, R. M., Kore, S. V, Kore, V. S., & Kulkarni, G. S. (2011). A Short Review on Process and Applications of Reverse Osmosis. *Universal Journal of Environmental Research and Technology*, *1*(3), 233–238.

González, D., Amigo, J., & Suárez, F. (2017). Membrane distillation: Perspectives for sustainable and improved desalination. *Renewable and Sustainable Energy Reviews*, *80*(April 2016), 238–259. https://doi.org/10.1016/j.rser.2017.05.078

Guo, A., Ming, X., Fu, Y., Wang, X. (2017). Fiber-based, double-sided, reduced graphene oxide films for efficient solar vapour generation. *ACS App*, *9*, 29958–29964. https://doi.org/https://doi.org/10.1021/acsami.7b07759

Guo, H., Li, X., Yang, W., Yao, Z., Mei, Y., Peng, L. E., Yang, Z., Shao, S., & Tang, C. Y. (2022). Nanofiltration for drinking water treatment: a review. *Frontiers of Chemical Science and Engineering*, *16*(5), 681–698. https://doi.org/10.1007/s11705-021-2103-5

Han, B., Runnellsb, T., Zimbronb, J., & Wickramasinghe, R. (2002). Arsenic removal from drinking water microfiltration. *Desalination*, *145*, 293–298. www.elsevier.com/locate/desal

Hashim, A. Y., Al-asadi, J. M., & Taha, W. a. (2009). Experimental investigation of symmetrical double slope single basin solar stills productivity with different Insulation. *Journal of Kufa – Physics*, *1*(2), 26–32.

Jakhar, M, Laura, J.S., Nandal, M. (2023). Nanofiltration membrane techniques for heavuy metal separation. In *modern nanotechnology* (pp. 301–327). Springer, Cham. https://doi.org/https://doi.org/10.1007/978-3-031-31111-6_13

Jiang, S., Zhang, Z., Zhou, T., Duan, S., Yang, Z., Ju, Y., Jia, C., Lu, X., & Chen, F. (2022). Lignin hydrogel-based solar-driven evaporator for cost-effective and highly efficient water purification. *Desalination*, *531*(January), 115706. https://doi.org/10.1016/j.desal.2022.115706

Johnson, D.J., Suwaileh, W.A., Mohammed, A.W., Hilal, N. (2017). Osmotic's potential: an overview of draw solutes for forward osmosis. *Desalination*. https://doi.org/10.1016/j.desal.2017.09.017

Jones, E., Qadir, M., van Vliet, M. T. H., Smakhtin, V., & Kang, S. mu. (2019). The state of desalination and brine production: A global outlook. *Science of the Total Environment*, *657*, 1343–1356. https://doi.org/10.1016/j.scitotenv.2018.12.076

Kabeel, A. E., Hamed, M. H., Omara, Z. M., & Sharshir, S. W. (2013). Water Desalination Using a Humidification-Dehumidification Technique—A Detailed Review. *Natural Resources*, *04*(03), 286–305. https://doi.org/10.4236/nr.2013.43036

Kelsey D.A. (2017). Where they tame the undrinkable Ocean. *Popular Science.* https://www.popsci.com/dubais-desalination-plant-photos/

Kershner, I. (2015). Aided by the Sea, Israel Overcomes an Old Foe: Drought. *The New York Times*.

Khalifa, A. J. N., & Hamood, A. M. (2009). Effect of insulation thickness on the productivity of basin type solar stills: An experimental verification under local climate. *Energy Conversion and Management*, *50*(9), 2457–2461. https://doi.org/10.1016/j.enconman.2009.06.007

Khan, Q., Maraqa, M., Mohamed, A. (2021). Chapter 17- Inland desalination: techniques, brine management, and environmental concerns. *Pollution Assessment for Sustainable Practices in Applied Sciences and Engineering*, 871–918. https://doi.org/https://doi.org/10.1016/B978-0-12-809582-9.00017-7

Khan, S. U. D., Khan, S. U. D., Danish, S. N., Orfi, J., Rana, U. A., & Haider, S. (2018). Nuclear Energy Powered Seawater Desalination. In *Renewable Energy Powered Desalination Handbook: Application and Thermodynamics*. Elsevier Inc. https://doi.org/10.1016/B978-0-12-815244-7.00006-4

Kuzmenko, A. B., Van Heumen, E., Carbone, F., & Van Der Marel, D. (2008). Universal optical conductance of graphite. *Physical Review Letters*, *100*(11), 1–5. https://doi.org/10.1103/PhysRevLett.100.117401

Lange, M. A. (2013). Renewable energy and water resources. In *Climate vulnerability* pp. 149–166. https://doi.org/https://doi.org/10.1016/B978-0-12-384703-4.00320-8

Li, X., Xu, W., Tang, M., Zhou, L., Zhu, B., Zhu, S., & Zhu, J. (2016). Graphene oxide-based efficient and scalable solar desalination under one sun with a confined 2D water path. *Proceedings of the National Academy of Sciences of the United States of America*, *113*(49), 13953–13958. https://doi.org/10.1073/pnas.1613031113

Li, Z., Wang, C., Lei, T., Ma, H., Su, J., Ling, S., & Wang, W. (2019). Arched Bamboo Charcoal as Interfacial Solar Steam Generation Integrative Device with Enhanced Water Purification Capacity. *Advanced Sustainable Systems*, *3*(4), 1–10. https://doi.org/10.1002/adsu.201800144

Liang, P., Liu, S., Ding, Y., Wen, X., Wang, K., Shao, C., Hong, X., Liu, Y. (2021). A self-floating electrospun nanofiber mat for continuously high-efficiency solar desalination. *Chemosphere*, *280*.

Liang, X., Pei, X., Yang, Y., Jia, E., Zhou, H., Xiang, S., Lin, F., & Tan, Y. (2022). A robust PVA/C/sponge composite hydrogel with improved photothermal interfacial evaporation rate inspired by the chimney effect. *Desalination*, *531*(March), 115720. https://doi.org/10.1016/j.desal.2022.115720

Liu, X., Shanbhag, S., Bartholomew, T. V., Whitacre, J. F., & Mauter, M. S. (2021). Cost Comparison of Capacitive Deionization and Reverse Osmosis for Brackish Water Desalination. *ACS ES&T Engineering*, *1*(2), 261–273. https://doi.org/10.1021/acsestengg.0c00094

Liu, Y., & Song, C. (2018). Bioinspired Materials in Evaporation. *Bioinspired Engineering of Thermal Materials*, 73–98. https://doi.org/10.1002/9783527687596.ch4

Ma, A., Chen, Y., Liu, Y., Gui, J., Yu, Y. (2020). Reduced graphene oxide/carbon fiber composite membrane for self-floating solar-thermal steam production. *Chemical Research in Chinese Universities*, *36*, 699–702.

Morris, R.M., Hanbury, W. T. (1991). Predication of critical desalination parameters using radial basis functions network. In *Proceedings of the new technologies for the use of renewable energy sources in water desalination.* (pp. 30–50).

Narayanan, S. S., Yadav, A., & Khaled, M. N. (2020). A concise review on performance improvement of solar stills. *SN Applied Sciences*, *2*(3), 1–15. https://doi.org/10.1007/s42452-020-2291-5

Ni, G., Li, G., Boriskina, S. V., Li, H., Yang, W., Zhang, T. J., & Chen, G. (2016). Steam generation under one sun enabled by a floating structure with thermal concentration. *Nature Energy*, *1*(9). https://doi.org/10.1038/nenergy.2016.126

Ni, G., Zandavi, S. H., Javid, S. M., Boriskina, S. V., Cooper, T. A., & Chen, G. (2018). A salt-rejecting floating solar still for low-cost desalination. *Energy and Environmental Science*, *11*(6), 1510–1519. https://doi.org/10.1039/c8ee00220g

Omara, Z. M., Abdullah, A. S., Kabeel, A. E., & Essa, F. A. (2017). The cooling techniques of the solar stills' glass covers – A review. *Renewable and Sustainable Energy Reviews*, *78*(March), 176–193. https://doi.org/10.1016/j.rser.2017.04.085

Ren, L., Yi, X., Yang, Z., Wang, D., Liu, L., & Ye, J. (2021). Designing carbonized loofah sponge architectures with plasmonic Cu nanoparticles encapsulated in graphitic layers for highly efficient solar vapor generation. *Nano Letters*, *21*(4), 1709–1715. https://doi.org/10.1021/acs.nanolett.0c04511

Sarkar, N., Tiwari, A. K., & Somwanshi, A. (2022). Enhancement of distillate output of solar still by cooling glass cover. *International Journal of Health Sciences*, *6*(June), 9400–9421. https://doi.org/10.53730/ijhs.v6ns5.9563

Shang, W., & Deng, T. (2016). Solar steam generation: Steam by thermal concentration. *Nature Energy*, *1*(9), 1–2. https://doi.org/10.1038/nenergy.2016.133

Sharon, H., & Reddy, K. S. (2015). A review of solar energy driven desalination technologies. *Renewable and Sustainable Energy Reviews*, *41*, 1080–1118. https://doi.org/10.1016/j.rser.2014.09.002

Sharshir, S. W., Yang, N., Peng, G., & Kabeel, A. E. (2016). Factors affecting solar stills productivity and improvement techniques: A detailed review. *Applied Thermal Engineering*, *100*, 267–284. https://doi.org/10.1016/j.applthermaleng.2015.11.041

Shatilla, Y. (2020). Nuclear desalination. In *Nuclear reactor technology development and utilization* (pp. 247–270). Elsevier Ltd. https://doi.org/https://doi.org/10.1016/C2018-0-04201-2

Shi, L., Wang, Y., Zhang, L., Wang, P. (2017). Rational design of a bi-layered reduced graphene oxide film on polystyrene foam for solar-driven interfacial evaporation. *Journal of Materials Chemistry A*, *5*, 16212–16219.

Tao, P., Ni, G., Song, C., Shang, W., Wu, J., Zhu, J., Chen, G., & Deng, T. (2018). Solar-driven interfacial evaporation. *Nature Energy*. https://doi.org/10.1038/s41560-018-0260-

7

Tiwari, G.N., Sahota, L. (2017). *Advanced solar-distillation systems: basic principles, thermal modelling, and its application.* Springer nature Singapore. https://doi.org/10.1007/978-981-10-4672-8

Tiwari, A. K., & Tiwari, G. N. (2007). Thermal modeling based on solar fraction and experimental study of the annual and seasonal performance of a single slope passive solar still: The effect of water depths. *Desalination*, *207*(1–3), 184–204. https://doi.org/10.1016/j.desal.2006.07.011

Tofighy, M. A., Mohammadi, T., & Sadeghi, M. H. (2021). High-flux PVDF/PVP nanocomposite ultrafiltration membrane incorporated with graphene oxide nanoribbones with improved antifouling properties. *Journal of Applied Polymer Science*, *138*(4), 1–15. https://doi.org/10.1002/app.49718

Utilities Middle East. (2018). Acciona Agua wins $232mn desalination contract in Saudi Arabia. https://www.utilities-me.com/power/11612-acciona-agua-wins-232mn-desalination-contract-in-saudi-arabia

Xu, W., Hu, X., Zhuang, S., Wang, Y. (2018). Flexible and salt resistant Janus absorbers by electrospinning for stable and efficient solar desalination. *Advanced Energy Materials*, *8*(14). https://doi.org/10.1002/aenm.201702884

Xu, Z., Zhang, L., Zhao, L., Li, B., Bhatia, B., Wang, C., Wilke, K. L., Song, Y., Labban, O., Lienhard, J. H., Wang, R., & Wang, E. N. (2020). Ultrahigh-efficiency desalination: Via a thermally-localized multistage solar still. *Energy and Environmental Science*, *13*(3), 830–839. https://doi.org/10.1039/c9ee04122b

Yan, J., Su, Q., Xiao, W., Wu, Z., Chen, L., Tang, L., Zheng, N., Gao, J., & Xue, H. (2022). A review of nanofiber membranes for solar interface evaporation. *Desalination*, *531*(180), 115686. https://doi.org/10.1016/j.desal.2022.115686.

Wagner, T. (2020). Policy instruments to reduce consumption of expanded polystyrene food service ware in the USA. *Detritus, Multidisciplinary Journal of Waste resources & residues. 9*, 11-26.

Zeng, Y., Yao, J., Hori, B., Wang, K., Wu, Y., Li, D., Wang, H. (2011). Solar evaporation enhancement using floating light-absorbing magnetic particles. *Energy and Environmental Science*, *4*, 4074–4078. https://doi.org/https://doi.org/10.1039/C1EE01532J

Zhang, Q., Yang, X., Deng, H., Zhang, Y., Hu, J., & Tian, R. (2022). Carbonized sugarcane as interfacial photothermal evaporator for vapor generation. *Desalination*, *526*, 115544. https://doi.org/10.1016/j.desal.2021.115544

Zhang, Y., Xiong, T., Nandakumar, D. K., & Tan, S. C. (2020). *Structure Architecting for Salt-Rejecting Solar Interfacial Desalination to Achieve High-Performance Evaporation With In Situ Energy Generation*. *1903478*. https://doi.org/10.1002/advs.201903478

Zhao, F., Guo, Y., Zhou, X., Shi, W., & Yu, G. (2020). Materials for solar-powered water evaporation. *Nature Reviews Materials*, *5*(5), 388–401. https://doi.org/10.1038/s41578-020-0182-4

Zhao, F., Zhou, X., Shi, Y., Qian, X., Alexander, M., Zhao, X., Mendez, S., Yang, R., Qu, L., & Yu, G. (2018). Highly efficient solar vapour generation via hierarchically nanostructured gels. *Nature Nanotechnology*, *13*(6), 489–495. https://doi.org/10.1038/s41565-018-0097-z

Zhuangzhi Sun, Wenzong Li, Wenlong Song, Laichang Zhang, Z. W. (2020). A high efficiency solar desalination evaporator composite of corn stalk, Mcnts and TiO2: ultra fast capillary water moisture transportation and porous bio-tissue multi layer filtration. *Journal of Materials Chemistry A*, *8*(1), 349–357.

Chapter 3

Materials and Methods

This chapter reports on the design of a single slope solar still, tyre dust paint preparation, evaporation structure preparation, wicking test on cellulose, insulation test on EPS and Extruded Polystyrene, process of freshwater collection, data collection on water samples before and after desalination, water hardness tests on water samples before and after desalination, and characterization procedures. In the design of a solar absorber, two methods were used. Method 1 was the coating of cellulose with tyre dust and EVA, and method 2 was the coating of cellulose with tyre dust in wheat flour paint. Method 2 was chosen over method 1 in this study because it exhibited a better rate of water absorption.

3.1 Material Sourcing

These are materials used for the preparation of tyre dust paint, evaporation structure, wicking test, water hardness test, and metal analysis.

Tyre dust powder used in this study was obtained from crumbled tyres acquired from a private recycling company located at Silverglen, Durban, South Africa, pure cellulose boards were provided by Council for Scientific and Industrial Research (CSIR) in Durban. Expanded and Extruded Polystyrene were recovered from packaging materials. EDTA, ammonium oxalate, ammonium chloride, aqueous ammonia, Eriochrome black T indicator were purchased from Merck. They were all analytical grades (AR) and were used without further purification. Metal standards were prepared from metal salts purchased from Merck.

3.1.1 Design of a single slope solar still

In this research, a single slope solar still as shown in Figure 3.1 was constructed. Pinewood was used for the construction of the solar still using a bottom area dimension of 550 mm by 550 mm. A glass sheet of 3 mm thickness was used as the condensation cover which was inclined at an angle of 20°. Linseed oil was used to initially coat the wood in order to protect it from insect attacks, harmful effect of humidity, and other deteriorating agents.

Layers of black coloured silicone were applied to the inner surface of the solar still to make the basin waterproof so as to prevent water leakage from the box. PVC taps were fixed at three different points for water inlet, water drainage, and freshwater collection from the trough/gutter pipe as shown in Figure 3.1. A clean plastic container for freshwater collection was connected to the gutter pipe using a clean hose.

Figure 3.1: Set-up of a solar still protoype capturing radiant solar energy on a roof top

3.1.2 Water samples

Four different water samples (Tap Water, Seawater, Synthetic Water (to mimic seawater), and Borehole water) were used in this study. Tap water was collected from the tap on the rooftop of H block, University of KwaZulu-Natal. Seawater was sampled from South Beach, Durban. The water sample was collected using 25 L x 2 plastic containers which were washed, rinsed with deionized water and finally rinsed twice with the seawater sample before collection. Synthetic water was prepared in the analytical laboratory (method of preparation will be outlined in the methods section). Borehole water was sourced from a farm in Shongweni, Durban. The pH and conductivity of the water samples were recorded using

Mettler Toledo Seven Excellence S470 pH/conductivity meter and then stored in the refrigerator at about 4°.

3.2 Methods

This section covers detailed outline of steps taken during the study. These include preparation of the solar absorber,

3.2.1 Preparation of the solar absorber

In preparing the solar absorber, different methods were used to achieve a porous solar absorber with a black surface.

3.2.1.1 Method 1: Pure cellulose coated with Tyre dust and EVA cross-linker

A mass of 10 g of tyre dust was mixed with an EVA cross-linker (34.599 g) to form a black slurry. Four pieces of pure cellulose, 1, 2, 3, and 4 with the same height and width were coated with the slurry by rubbing the slurry on both sides of paper 1, rubbing one side of paper 2, dabbing both sides of paper 3 and dabbing one side of paper 4 and they were then allowed to dry at room temperature. Upon drying, a water absorption test was carried out on each sample paper. A beaker was filled with water and each of the coated samples was placed on the water to see which would absorb water while remaining afloat. Sample 1 stayed afloat and absorbed water at a very slow rate, sample 2 sank in the water immediately, sample 3 stayed afloat and absorbed water at a slow rate but faster than sample 1, and sample 4 sank as well. From this experiment, it was observed that samples 1 and 3 floated as a result of coating both sides of the paper while 2 and 4 sank as a result of coating only the top of the paper. Samples 1 and 3 also floated while absorbing water at a very slow rate as a result of the EVA cross-linker which tends to be hydrophobic.

3.2.1.2 Method 2: Pure cellulose coated with tyre dust and wheat flour paint.

The quantity of tyre dust paint produced was enough to coat a cellulose board of 540 mm^2

The following are the materials used: wheat flour 125 g; table salt 38 g; glycerol 38 mL; tyre dust 100 g; water 240 mL; beakers; glass rod stirrer; digital weighing balance and measuring cylinders.

3.2.2 Method of preparation of the wheat flour paint

A mass of 125 g of wheat flour was accurately weighed and transferred into a 200 mL beaker. A mass of 38 g of table salt (NaCl) was added and, the mixture was stirred. With the aid of a measuring cylinder, an accurately measured volume of 240 mL of deionized water was added gradually and the resulting mixture was stirred using a glass rod to form a smooth consistency. Glycerol was then added to the mixture and stirred vigorously to ensure the formation a homogenous mixture.

After preparation of the wheat flour paint, the cellulose board was painted with a brush on one side and allowed to air dry.

3.2.3 Preparation of the wicking structure

Pure cellulose was used as the wicking material in this experiment and it was chosen because of its porosity, low-cost, high level of purity, and availability. The cellulose boards were cut into smaller sizes (80 mm x 40 mm), dipped into deionized water, taken out, and flapped to increase their foldability. The wet cellulose was then folded to cylindrical shapes and allowed to dry.

3.2.3.1 Capillary/wicking test on cellulose

To test the capillary/wicking ability in the vertical direction, cellulose paper 120 mm in length was placed in an aqueous solution containing purple dye to observe the absorption and movement of moisture through the cellulose paper.

A cellulose paper of 1 mm thickness and 120 mm length was cut and marked with a pencil. It was placed in a beaker containing purple dye solution and observed for 60 minutes. The result gotten is shown and explained in Section 4.4.

3.2.4 Preparation of the insulation material

In choosing an insulation material, different criteria were looked at which included its ability to remain afloat, material stability after a long period, ability to block the heat from getting to the bulk water. Polystyrene was eventually chosen because of its mechanical rigidity in water, cost-effectiveness and most of all, its hydrophobic nature that makes it resistant to degradation. It is a good insulator because of its low thermal conductivity and it floats

because of its low density. Expanded polystyrene was obtained from packaging boxes and was dismantled by cutting. It was drilled to create several holes in it in order to allow the passage of the cellulose wicks since it lacks its own ability to absorb liquid at a fast rate. The polystyrene boards were then washed to get rid of dust and stains that could be a source of external contamination to the water samples and allowed to dry. The folded cellulose boards were then inserted into the drilled holes of the polystyrene. The parts above the polystyrene were tweezed to deliver more water to the surface.

3.2.4.1 Insulation test on EPS and Extruded Polystyrene

In order to determine the best type of polystyrene for interfacial evaporation, an insulation test was carried out on EPS and Extruded Polystyrene.

3.2.4.2 Materials and method

The materials used for this experiment include: water; temperature sensors; solar still (2); expanded polystyrene (EPS); extruded polystyrene; solar energy.

The method used is outlined below:

A volume of 20 L of water was poured into each of the two different solar stills, EPS and Extruded Polystyrene were drilled, and cellulose paper was fitted into the drilled holes to block the bulk water from direct sunlight that would pass through the holes and also wick up water to the surface of the polystyrene. EPS and Extruded Polystyrene boards as shown in figure 3.2 and figure 3.3 were then placed on each of the water surfaces. Temperature sensors were dipped into the water underneath the polystyrene boards and temperature readings were taken at an hour intervals for six hours. The result is explained graphically in Figure 4.7.
Figure 3.4 (a) is a pictorial representation showing the strands of pure cellulose passed through the drilled holes of the expanded polystyrene. The EPS board was placed directly on the water surface in the solar still and ensured that the entire surface of the water was covered by it. Figure 3.4 (b) shows the solar absorber placed on (a) which is the EPS board and the wicks. By placing the solar absorber on it, the sun only gets to heat it directly while the wicks draw up water. The water underneath the EPS remained unheated because of the low thermal conductivity of the EPS.

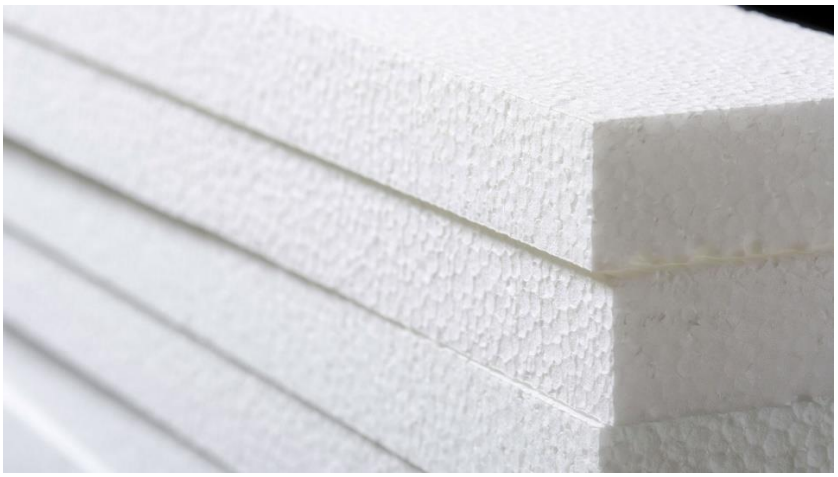

Figure 3.2: Image of expanded polystyrene.

Figure 3.3: Image of extruded polystyrene

Figure 3.4: Image of the development of the evaporation structure in a solar still showing (a) insulator and wicking structure made of cellulose. (b) solar absorber placed on the wicking structure and temperature sensors.

3.3 Preparation of synthetic water sample (to mimic seawater)

Forty litres of synthetic water was prepared using the following materials:

- Deionized water (pH and conductivity of 7.105 and 0.2 µS/cm respectively)
- 1132.8 g of sodium chloride (NaCl)
- 219.2 g of magnesium chloride hexahydrate ($MgCl_2.6H_2O$)
- 144 g of magnesium sulphate ($MgSO_4$)
- 44.4 g of calcium chloride dihydrate ($CaCl_2.2H_2O$)
- 30.8 g of potassium chloride (KCl)
- 8 g of sodium bicarbonate ($NaHCO_3$) (Nguyen, 2018).

Accurately weighed salts was added to a deionized water and stirred until the salts were fully dissolved, homogenized and made up to a known volume with deionized water. The pH, conductivity, TDS and salinity of the prepared sample were recorded. The sample was then stored in clean plastic containers.

3.4 Process of desalination and preparation of desalinated water from tap, sea, synthetic, and borehole water samples

The volume of water was collected on different days at different weather conditions, that can be considered “sunny” and “cloudy” days .

The solar still and trough were always first washed with deionized water to get rid of external contaminants and then lined with black plastic bag that served as extra waterproof and at the same time, prevented the silicone initially used as waterproof from polluting the water in the box. A volume of 40 L of water sample was poured into the box. The photothermal materials were then placed on the surface of the water. The trough was cleaned to get rid of any water sample or material that may have fallen into it during the process of filling and placing the photothermal materials. Four temperature sensors were placed at strategic positions in the box which are i) inside the bulk water, ii) in the wicking structure, iii) underneath the solar absorber, and iv) on the solar absorber. The inner and outer surface of the glass cover was washed, rinsed and dried with a clean cloth to get rid of external contaminants such as dust and water on its surface. The glass cover was then placed on the solar still to allow the condensation of the produced vapour. A plastic hose was washed with deionized water and fixed tightly to the tap of the solar still which collected the freshwater from the trough into a plastic bottle.

The volume of freshwater collected on each day was measured, and its physical parameters: pH, conductivity, total dissolved solids, and salinity were recorded using a RS232 Conductivity meter AZ 8306 and Mettler Toledo Seven excellence multiparameter S470 pH/conductivity meter. The data gotten from the physical parameters of water samples measured before and after desalination are shown in tables 3.1 and 3.2.

3.5 Determination of Total Dissolved Solid (TDS)

The determination of TDS was carried out in a clean glass beaker which was cleaned and properly dried and then weighed using a digital weighing balance. 25 mL of the water sample was then poured into the beaker and placed on the electric hot plate to evaporate the water to dryness. After evaporation, the beaker was removed from the hot plate and allowed to cool (Musyoka 2012). The mass of the cooled empty beaker was then taken.

3.6 Water hardness tests on water samples before and after desalination

Reagents:

The following reagents were used in tests for water hardness before and after desalination.

- Aqueous ammonia/ammonium chloride (0.2 M NH_3(aq)/0.2 M NH_4Cl) buffer at pH 10.
- Eriochrome black-T indicator
- 0.01M ethylenediaminetetraacetic acid (EDTA)
- Saturated ammonium oxalate solution
- Water samples

Total hardness:

A 50 mL aliquot of water sample was transferred into a conical flask to which 2.0 mL of a pH 10 buffer solution and 4 drops of EBT indicator were added. The water sample was titrated against a standard 0.01 M EDTA solution to an EBT end point of wine red to pure blue. The titration was was repeated until three concordant values were obtained. (UKZN Environmental Chemistry Practical Manual, 2023).

Permanent hardness:

A volume of 250 mL of the water sample was gently boiled in a 600 mL beaker for 20-30 minutes. It was then cooled and filtered into a 250 mL volumetric flask to remove the precipitated bicarbonates, and then made up to the mark with deionized water. The solution was then homogenized and 50 mL portion of it was taken and titrated with using the same procedure as total hardness. (UKZN Environmental Chemistry Practical Manual, 2023).

Temporary hardness:

This was gotten for each sample by the subtraction of permanent hardness from total hardness. (UKZN Environmental Chemistry Practical Manual, 2023).

3.7 Calculation of total hardness of water samples

Equation for the complexation reaction of Ca with EDTA (tetraanion):

$$CaCO_3 + EDTA^{4-}_{(aq)} \rightarrow Ca(EDTA)^{2-}_{(aq)} + CO^{2-}_{3\ (aq)} \quad \text{.....(4)}$$

Based on a reacting molar ratio of 1:1 for $CaCO_3$: $EDTA^{4-}$

The amount of $CaCO_3$ is calculated and subsequent total hardness determined.

Total hardness (expressed as total $CaCO_3$ mg/dm^3) = Conc of $CaCO_3$ mol/dm^3 x molar mass of $CaCO_3$ x 1000 mg/g.

3.8 Salinity

Samples were filtered and the levels of salinity were measured using RS232 Conductivity/Salinity meter AZ 8306.

3.9 Characterisations of the materials used in the development of the evaporation structure

The surface morphology and structure of the pure cellulose and tyre dust powder were studied by scanning electron microscopy using a Carl Zeiss Ultra Plus, and compared with the SEM images of the coated cellulose.

The nature of chemical bonding was analyzed by Fourier-transform infrared (FTIR), Perkin Elmer series 100 spectrometer attached with an attenuated total reflectance (ATR).

3.10 Metal analysis of water by ICP-OES

Metal analysis using ICP-OES (Perkin Elmer Optima 5300 DV) was carried out on the water samples and freshwater samples collected on different days.

3.10.1 Sample preparation

The following were carried out on the water samples before taking to the ICP-OES for analysis. The samples were acidified to ensure that their elemental components remained in solution before being taken for analysis.

3.10.1.1 Acidification of water samples

This was carried out to ensure the analytes were readily available in the sample solution.

Reagents

- Deionized water
- Concentrated nitric acid

- Water samples.

Process of sample preconcentration and acidification

A portion of 50 mL of the water sample was pipetted into a 100 mL beaker and 5 mL of conc entrated nitric acid was added to it. The solution was heated on an electric hot plate until the volume was reduced to about 30 mL. It was allowed to cool and filtered under gravity into a 50 mL volumetric flask. The beaker and filter paper were then rinsed with 5 mL of deionized water and the volumetric flask was made up to the mark with deionized water. The liquid was homogenized and filtered through a 0.45 μm syringe filter and then analyzed using ICP-OES (Environmental Analysis Practical Manual, 2023).

The correlation intensity scans were obtained using the ICP-OES.

References

UKZN Environmental Chemistry Practical Manual. APCH 211. 2023. Hardness and Alkalinity of Water. Pp. 18-20

UKZN Environmental Analysis Practical Manual. APCH 332. 2023. Total Metal Content in Water:Acid Digestion. Pp. 28-29.

Musyoka, S.M. (2012). PhD thesis. P. 134. University of KwaZulu Natal.

Nguyen, T.V. (2018). Preparation of Artificial Seawater (ASW). Aquaculture Biotechnology Group, School of Science. Auckland University of Technology (AUT): Auckland.

Chapter 4

Results and Discussion: Interfacial Evaporation and Physicochemical Parametres of Water Samples

In this chapter, the results of the study is presented and discussed. The results are presented for each of the four water samples tap water, synthetic water, seawater, and borehole water. Also, a variation of observations during winter (July – August) and summer (September – November) were reported.

4.1 Freshwater collection via interfacial evaporation

Rooftop experiments were conducted during the winter (July - August) and summer (September - November) seasons on both sunny and cloudy days.

4.1.1 Sampling during winter

During the winter season, the experiments were carried out with the evaporation structures and without the evaporation structures on both sunny and cloudy days. Without the evaporation structure, on a cloudy day, no water was collected, and on a sunny day, an average of 30 mL of water was collected. With the evaporation structure, on a cloudy day, no water was collected, while on a sunny day, an average of 700 mL of water was collected.

4.1.2 Sampling during summer

During the summer season, experiments were carried out between September and November 2023. The experiments were also carried out with the evaporation structures and without the evaporation structures on both sunny and cloudy days. Without the evaporation structure, on a cloudy day, an average of 50 mL was collected. While on a sunny day, an average of 150 mL was collected. With the evaporation structure, on a cloudy day, about 40 mL of water was collected. On a sunny day, an average of 1000 mL was collected.

The use of the designed evaporation structure causes condensation to start within 10 minutes, and by 15 minutes, condensation occurs properly and vapour starts to form on the inner glass surface as shown in Figure 4.1. In 20 minutes, droplets of water start to form on the glass and

within an hour, these water droplets start to form water beads and trickle down the glass, and are then collected by the well cleaned and positioned trough.

The water collected from the trough is then taken for various analysis such as water hardness test. Physicochemical properties such as pH, conductivity, total dissolved solids (TDS), and salinity, and then metal ion concentration using ICP-OES.

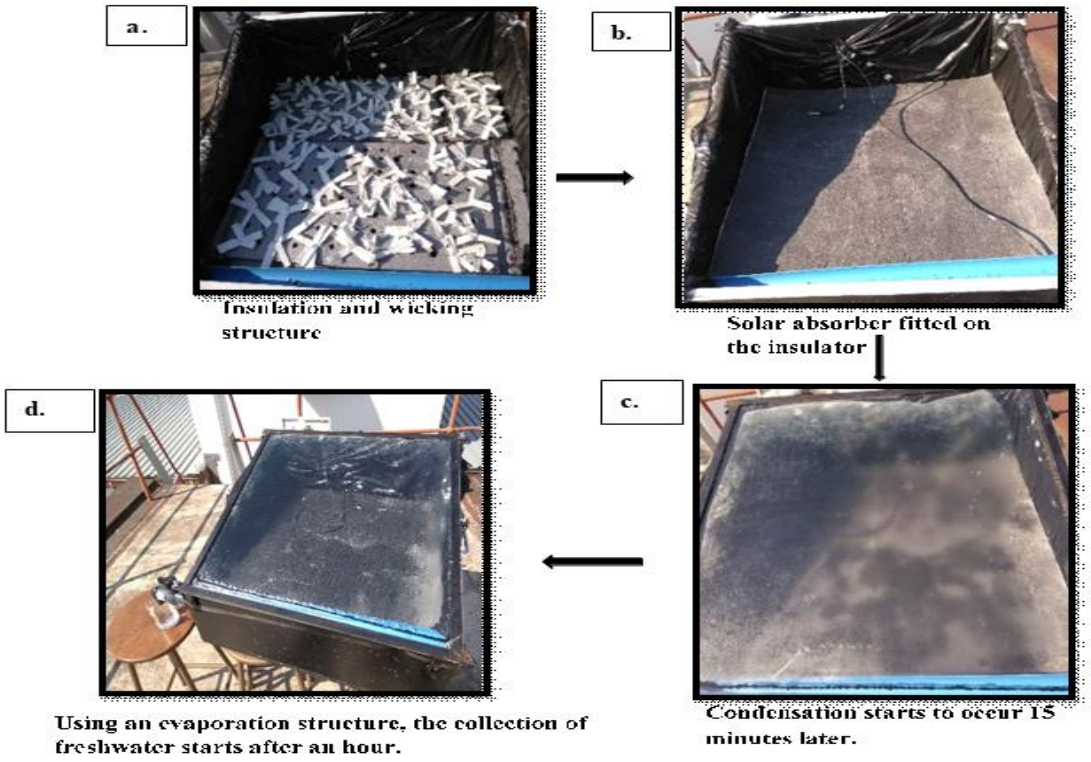

Figure 4.1: Preparation of the photothermal materials for desalination

4.2 Capillary/wicking test result

To test the capillary/wicking ability of the cellulose in the vertical direction, a 12 cm height of cellulose board was placed (0.5 cm depth) in an aqueous solution containing a purple dye to observe the rate of absorption and movement of moisture through the cellulose paper. In 1 minute, the dye was seen to go up the wick by 3.7 cm, and after 15 minutes, half of the cellulose had already been reached by the dye. After an hour, the dye was still observed to be moving up the cellulose. This experiment proves that cellulose is an excellent wicking material for this research as it allows for continuous wicking and it provides a 2D water pathway for interfacial evaporation.

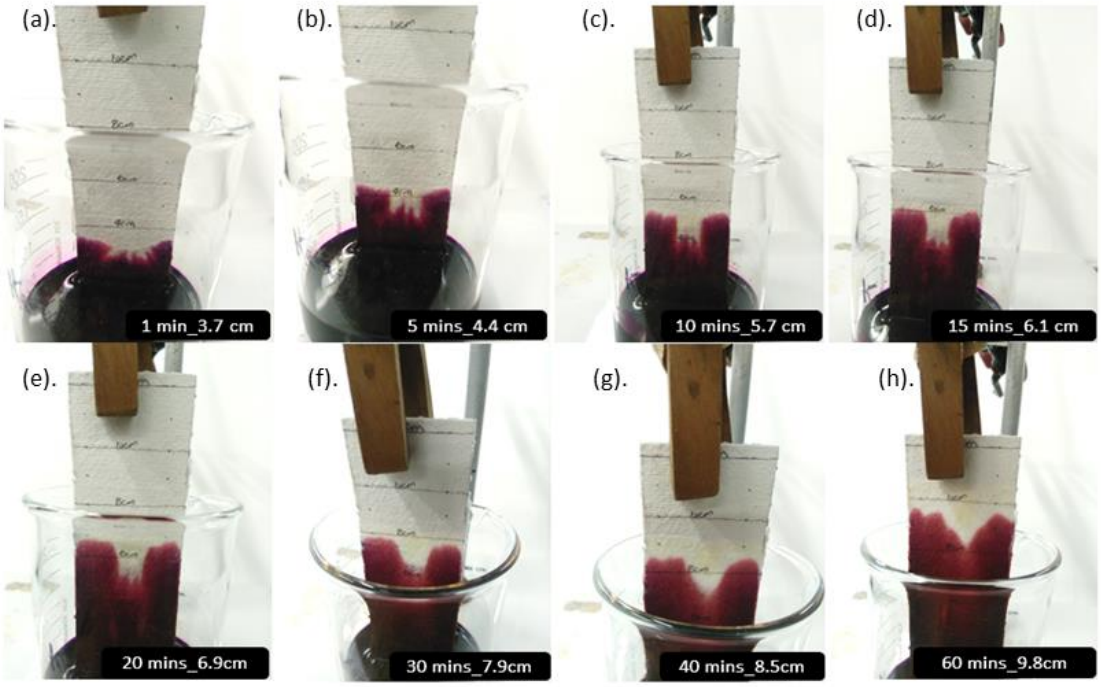

Figure 4.2: Capillary /wicking test on cellulose for a period of 60 minutes. Wicking time: (a) 1min, (b) 5mins, (c) 10 mins, (d) 15 mins, (e) 20 mins, (f) 30 mins, (g) 40 mins (h) 60 mins.

4.3 Insulation testing of the solar still using EPS and Extruded Polystyrene

From Figure 4.3, the temperatures of the water beneath the Extruded Polystyrene and EPS showed a gradual increase but remained cold even after hours of insolation. The temperature of Extruded Polystyrene was slightly greater than that of EPS. This shows that the temperature of the water underneath the Extruded Polystyrene increased while that underneath the EPS remained lower.

From this experiment, it can be deduced that EPS is the most suitable polystyrene for interfacial evaporation as the bulk water remained cooler than that underneath the Extruded Polystyrene.

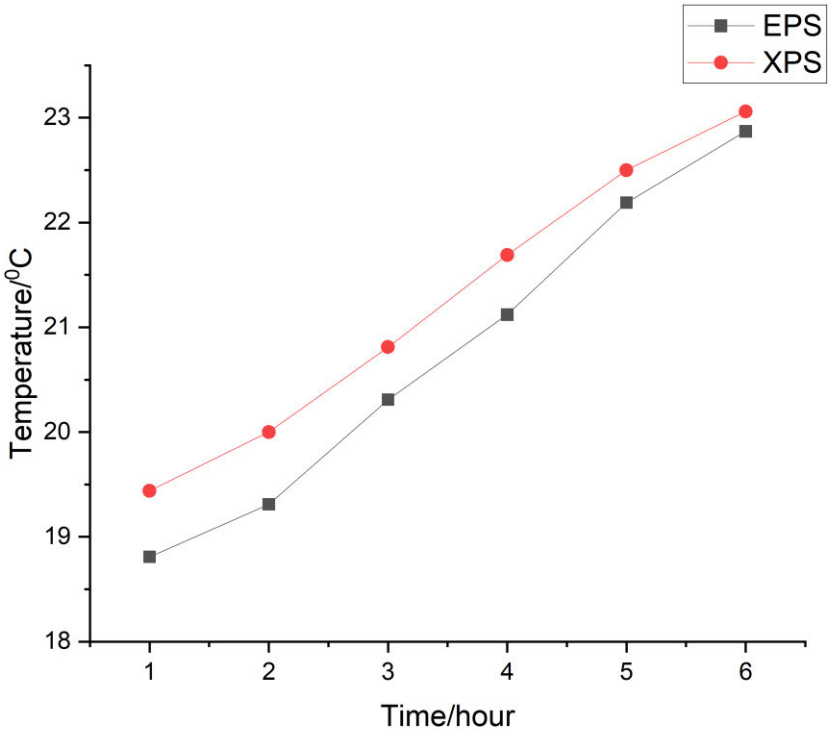

Figure 4.3: Temperature-time graph illustrating the increase in temperature of water beneath extruded polystyrene and expanded polystyrene in a solar still as shown in Figure 3.4.

4.4 Water hardness results and calculations

This was done using complexometric titration in which the formation of a coloured complex denotes the end point of the titration.

The concentration of calcium and magnesium ions in the water samples were determined by titrating 50 mL of the water samples with standard EDTA solution and Eriochrome Black T (EBT) indicator which shows the endpoint of the reaction. The EBT indicator formed complex with the Calcium and Magnesium ions in the water samples and formed a red coloured solution. On addition of EDTA to the solution, new complexes were formed with the calcium and magnesium ions because of the greater affinity between the EDTA and the complexes which is greater than that between the complexes and the EBT indicator. The red solution changed to blue when all the complexes were completely linked to the EDTA. Tables 4.1, 4.3, 4.5, 4.7, 4.9, 4.11, and 4.13 show the result for total hardness of the water samples before and after desalination. Tables 4.2, 4.4, 4.6, 4.8, 4.10, 4.12, and 4.14 show the result of permanent and temporary hardness of the water samples before and after desalination. Run 1, 2, and 3 indicate that titration of each water sample was done in triplicate

in order to ensure accuracy. As expected, the total hardness of each water sample was the sum of the permanent and temporary hardness.

The following sections discuss the titration results of the hardness tests performed on the four water samples.

4.4.1 Total hardness of Tap Water sample before desalination

Table 4.1: Complexometric titrations for total hardness of tap water showing titre volumes of standard EDTA solutions vs tap water samples before desalination at an EBT endpoint

Titre volume (cm^3) of Std EDTA at EBT endpoint	Run 1 (cm^3)	Run 2 (cm^3)	Run 3 (cm^3)	Average (cm^3)	Standard deviation
	2.30	2.35	2.35	2.33	$\pm$ 0.029 cm^3
Conc of $CaCO_3$ (M)	0.00047				
Total hardness (mg/L)	47.041				

Table 4.1 shows the result for total hardness of tap water before desalination which was calculated to be 47.041 mg/L indicating a slightly hard water.

Table 4.2: Complexometric titrations for permanent and temporary hardness of tap water showing titre volumes of standard EDTA solutions vs tap water samples before desalination at an EBT endpoint

Titre volume (cm^3) of Std EDTA at EBT endpoint	Run 1 (cm^3)	Run 2 (cm^3)	Run 3 (cm^3)	Average (cm^3)	Standard deviation
	2.30	2.45	2.30	2.35	± 0.087 cm^3
Conc of $CaCO_3$ (M)	0.00046				
Permanent hardness (mg/L)	46.040				
Temporary hardness (mg/L)	1.0008				

Table 4.2 is the result for permanent and temporary hardness of tap water which is 46.040 and 1.0008 mg/L before desalination. The sum total of the permanent and temporary hardness gives the total hardness.

4.4.2 Total hardness of Tap Water sample after desalination

Table 4.3: Complexometric titrations for total hardness of tap water showing titre volumes of standard EDTA solutions vs tap water samples after desalination at an EBT endpoint

Titre volume (cm^3) of Std EDTA at EBT endpoint	Run 1 (cm^3)	Run 2 (cm^3)	Run 3 (cm^3)	Average (cm^3)	Standard deviation
	0.20	0.40	0.40	0.40	± 0.115 cm^3
Conc of $CaCO_3$ (M)	0.00008				
Total hardness (mg/L)	8.0070				

The total hardness of tap water after desalination as seen in table 4.3 is 8.007 mg/L which indicates soft water. This is as a result of desalination as it removes salts and contaminants from water.

Table 4.4: Complexometric titrations for temporary and permanent hardness of tap water showing titre volumes of standard EDTA solutions vs tap water samples after desalination at an EBT endpoint

Titre volume (cm^3) of Std EDTA at EBT endpoint	Run 1 (cm^3)	Run 2 (cm^3)	Run 3 (cm^3)	Average (cm^3)	Standard deviation
	0.35	0.40	0.35	0.35	$\pm$ 0.029cm^3
Conc of $CaCO_3$ (M)	0.00007				
Permanent hardness (mg/L)	7.006				
Temporary hardness (mg/L)	1.0008				

In table 4.4, the values of permanent and temporary hardness are 7.006 and 1.0008 mg/L respectively which sums up to the value of total hardness.

4.4.3 Total hardness of Seawater sample before desalination

Table 4.5: Complexometric titrations for total hardness of seawater showing titre volumes of standard EDTA solutions vs seawater samples before desalination at an EBT endpoint

Titre volume (cm^3) of Std EDTA at EBT endpoint	Run 1 (cm^3)	Run 2 (cm^3)	Run 3 (cm^3)	Average (cm^3)	Standard deviation
	3.30	3.30	3.25	2.28	$\pm$ 0.029cm^3
Conc of $CaCO_3$ (M)	0.000656				
Total hardness (mg/L)	6565.70				

Table 4.5 is the result of total hardness for seawater sample before desalination which was calculated to be 6565.70 mg/L. This result shows the high salinity of seawater which is also an indication of it being a very hard water. The level of this hardness of seawater is extremely high which makes the water unfit for domestic, agricultural activities, and consumption.

Table 4.6: Complexometric titrations for permanent and temporary hardness of seawater showing titre volumes of standard EDTA solutions vs seawater samples before desalination at an EBT endpoint

Titre volume (cm^3) of Std EDTA at EBT endpoint	Run 1 (cm^3)	Run 2 (cm^3)	Run 3 (cm^3)	Average (cm^3)	Standard deviation
	3.10	3.15	3.15	3.13	$\pm$ 0.029cm^3
Conc of $CaCO_3$ (M)	0.0006267				
Permanent hardness (mg/L)	6272.106				
Temporary hardness (mg/L)	293.595				

Table 4.6 shows the temporary and permanent hardness of seawater before desalination to be 293.595 and 6272.106 mg/L which are summed up to give the total hardness gotten in table 4.5.

4.4.4 Total hardness of Seawater sample after desalination

Table 4.7: Complexometric titrations for total hardness of seawater showing titre volumes of standard EDTA solutions vs seawater samples after desalination at an EBT endpoint

Titre volume (cm^3) of Std EDTA at EBT endpoint	Run 1 (cm^3)	Run 2 (cm^3)	Run 3 (cm^3)	Average (cm^3)	Standard deviation
	1.80	0.80	0.80	0.80	± 0.577 cm^3
Conc of $CaCO_3$ (M)	0.00016				
Total hardness (mg/L)	16.0139				

Table 4.7 shows the result of the total hardness of seawater after desalination to be 16.0139 mg/L. There is a large difference between the total hardness before desalination as shown in table 4.5 and after desalination which is a proof that the solar still is a good technique for desalination.

Table 4.8: Complexometric titrations for permanent and temporary hardness of seawater showing titre volumes of standard EDTA solutions vs seawater samples after desalination at an EBT endpoint

Titre volume (cm^3) of Std EDTA at EBT endpoint	Run 1 (cm^3)	Run 2 (cm^3)	Run 3 (cm^3)	Average (cm^3)	Standard deviation
	0.75	0.65	0.65	0.65	± 0.058 cm^3
Conc of $CaCO_3$ (M)	0.00013				
Permanent hardness (mg/L)	13.011				
Temporary hardness (mg/L)	3.003				

Table 4.8 represents the permanent and temporary hardness of seawater sample after desalination to be 13.011 and 3.003 mg/L.

4.4.5 Synthetic Water sample before desalination

Table 4.9: Complexometric titrations for total hardness of synthetic water showing titre volumes of standard EDTA solutions vs synthetic water samples before desalination at an EBT endpoint

Titre volume (cm^3) of Std EDTA at EBT endpoint	Run 1 (cm^3)	Run 2 (cm^3)	Run 3 (cm^3)	Average (cm^3)	Standard deviation
	3.00	3.15	3.05	3.08	cm^3
Conc of $CaCO_3$ (M)	0.00062				
Total hardness (mg/L)	6205.39				

Table 4.9 represents the total hardness of synthetic water before desalination. The total hardness calculated being 6205.39 mg/L indicates a very hard water which is close to that of seawater as shown in table 4.5. This shows that the synthetic water was well prepared to mimic the seawater.

Table 4.10: Complexometric titrations for permanent and temporary hardness of synthetic water showing titre volumes of standard EDTA solutions vs synthetic water samples before desalination at an EBT endpoint

Titre volume (cm^3) of Std EDTA at EBT endpoint	Run 1 (cm^3)	Run 2 (cm^3)	Run 3 (cm^3)	Average (cm^3)	Standard deviation
	2.55	2.75	2.80	2.78	$\pm$ 0.076 cm^3
Conc of $CaCO_3$ (M)	0.000555				
Permanent hardness (mg/L)	5554.823				
Temporary hardness (mg/L)	650.567				

Table 4.10 shows the permanent and temporary hardness of synthetic water before desalination to be 5554.823 and 650.567 mg/L respectively.

4.4.6 Synthetic Water sample after desalination

Table 4.11: Complexometric titrations for total hardness of synthetic water showing titre volumes of standard EDTA solutions vs synthetic water samples after desalination at an EBT endpoint

Titre volume (cm^3) of Std EDTA at EBT endpoint	Run 1 (cm^3)	Run 2 (cm^3)	Run 3 (cm^3)	Average (cm^3)	Standard deviation
	0.25	0.20	0.20	0.20	$\pm$ 0.029cm^3
Conc of $CaCO_3$ (M)	0.00004				
Total hardness (mg/L)	4.0035				

Table 4.11 shows the total hardness of synthetic water sample after desalination to be 4.0035 mg/L indicating soft water. This massive drop of hardness after desalination is a proof that solar desalination is indeed a good water purification technique.

Table 4.12: Complexometric titrations for permanent and temporary hardness of synthetic water showing titre volumes of standard EDTA solutions vs synthetic water samples after desalination at an EBT endpoint

Titre volume (cm^3) of Std EDTA at EBT endpoint	Run 1 (cm^3)	Run 2 (cm^3)	Run 3 (cm^3)	Average (cm^3)	Standard deviation
	0.15	0.25	0.10	0.13	± 0.076 cm^3
Conc of $CaCO_3$ (M)	0.000025				
Permanent hardness (mg/L)	2.502				
Temporary hardness (mg/L)	1.5015				

Table 4.12 is the result for permanent and temporary hardness of synthetic water being 2.502 and 1.5015 mg/L.

4.4.7 Borehole Water sample before desalination

Table 4.13: Complexometric titrations for total hardness of borehole water showing titre volumes of standard EDTA solutions vs borehole water samples before desalination at an EBT endpoint

Titre volume (cm^3) of Std EDTA at EBT	Run 1 (cm^3)	Run 2 (cm^3)	Run 3 (cm^3)	Average (cm^3)	Standard deviation

endpoint	1.05	1.25	1.25	1.25	± 0.115 cm^3
Conc of $CaCO_3$ (M)	0.00025				
Total hardness (mg/L)	2502.1725				

Table 4.13 shows the total hardness of borehole water sample before desalination to be 2502.1725 mg/L which indicates a very hard water. This was expected as the water sample was seen to be highly impure and unfit for drinking.

Table 4.14: Complexometric titrations for permanent and temporary hardness of borehole water showing titre volumes of standard EDTA solutions vs borehole water samples before desalination at an EBT endpoint

Titre volume (cm^3) of Std EDTA at EBT endpoint	Run 1 (cm^3)	Run 2 (cm^3)	Run 3 (cm^3)	Average (cm^3)	Standard deviation
	1.45	1.20	1.20	1.20	± 0.144 cm^3
Conc of $CaCO_3$ (M)	0.00024				
Permanent hardness (mg/L)	2402.1				
Temporary hardness (mg/L)	100.0725				

4.4.8 Borehole water after desalination

On addition of Eriochrome black T indicator to the water sample, there was no endpoint color change observed. This could be as a result of the absence of Ca^{2+} and Mg^{2+} in the water sample. It can thus be concluded that Ca^{2+} and Mg^{2+} were completely removed after desalination. This precision of the result was confirmed by performing the titration in triplicate which produced the same result each time.

From the total water hardness calculation above, it is evident that the hardness of each water sample decreased substantially, especially after desalination.

Eriochrome black T was used as an indicator in this titration because it forms a complex with Ca^{2+} , Mg^{2+}, and other metal ions in its protonated form giving a wine-red color. On addition

of EDTA, the metal ion complexed with EBT is replaced with EDTA because EDTA has a greater affinity than EBT. The end point of this titration gave a blue coloration which indicated that EBT returned to its uncomplexed color.

Aqueous ammonia/ammonium chloride (0.2 M $NH_{3(aq)}$)/0.2 M NH_4Cl buffer with pH 10 was used to ensure consistent results of titrations by controlling the pH of the solutions.

Water hardness can be classified into various categories. According to the WHO, water with total hardness less than 17 mg/L is regarded as soft water, while within the range of 17-60 mg/L is slightly hard. When the total hardness is within the range of 60-120 mg/L it is said to be morderately hard. It is considered to be very hard when the total hardness is greater than 180 mg/L. Table 4.15 shows the water hardness classification of the water samples before and after desalination.

Table 4.15: Classification of the type of hardness of tap water samples based on the determination of total hardness

Water samples	**Salination treatment procedure**	**Total hardness (ppm)**	**Hardness classification**
1. Tap water	Before	47.04	Slightly hard water
2. Tap water	After	8.01	Soft water
3. Seawater	Before	6565.70	Very hard water
4. Seawater	After	16.01	Soft water
5. Synthetic water	Before	6205.39	Very hard water
6. Synthetic sea	After	4.00	Soft water
7. Borehole	Before	2502.17	Very hard water
8. Borehole water	After	No hardness detected	Soft water

From the table above, it can be seen that after desalination, the extremely hard water samples were converted to soft water.

4.5 Results of the Physicochemical parameters of Water Samples before and after Desalination Treatment

These results include pH, electrical conductivity, total dissolved solids, and salinity of the water samples before and after desalination. Tables 4.16 and 4.17 show the data gotten from the analysis of the water samples.

Table 4.16: Chemical and physical parameters of water samples before desalination.

Water samples	**pH**	**Conductivity/µS/cm**	**TDS/ppm**	**Salinity/ppt**	**Temperature (°C)**
Tap water	7.65	0.80	40.00	2.00	19.60
Seawater	8.33	237.10	24280.00	30.60	19.60
Synthetic water	8.36	203.00	20680.00	25.50	21.10
Borehole water	4.67	52.85	52720.00	6.40	21.70

Table 4.17: Chemical and physical parameters of water samples after desalination.

Water samples	**pH**	**Conductivity/µS/cm**	**TDS/ppm**	**Salinity/ppt**	**Temperature (°C)**
Tap water	7.11	0.20	40.00	2.00	21.00
Seawater	7.97	0.80	120.00	2.00	22.00
Synthetic water	7.88	0.30	80.00	2.00	24.10
Borehole water	7.74	0.30	45120.00	2.00	21.80

4.5.1 pH

The average pH values of the four water samples were measured using Hanna edge H12020. The measurements were carried out in triplicates, recorded, and the average was calculated and used. Figure 4.4 is a graphical representation of the pH values of the water samples before and after desalination. Before desalination, the values for tap water, synthetic water,

seawater, and borehole water were 7.65, 8.33, 8.36, and 4.67 respectively. After desalination, the values became 7.11, 7.97, 7.88, and 7.74 respectively.

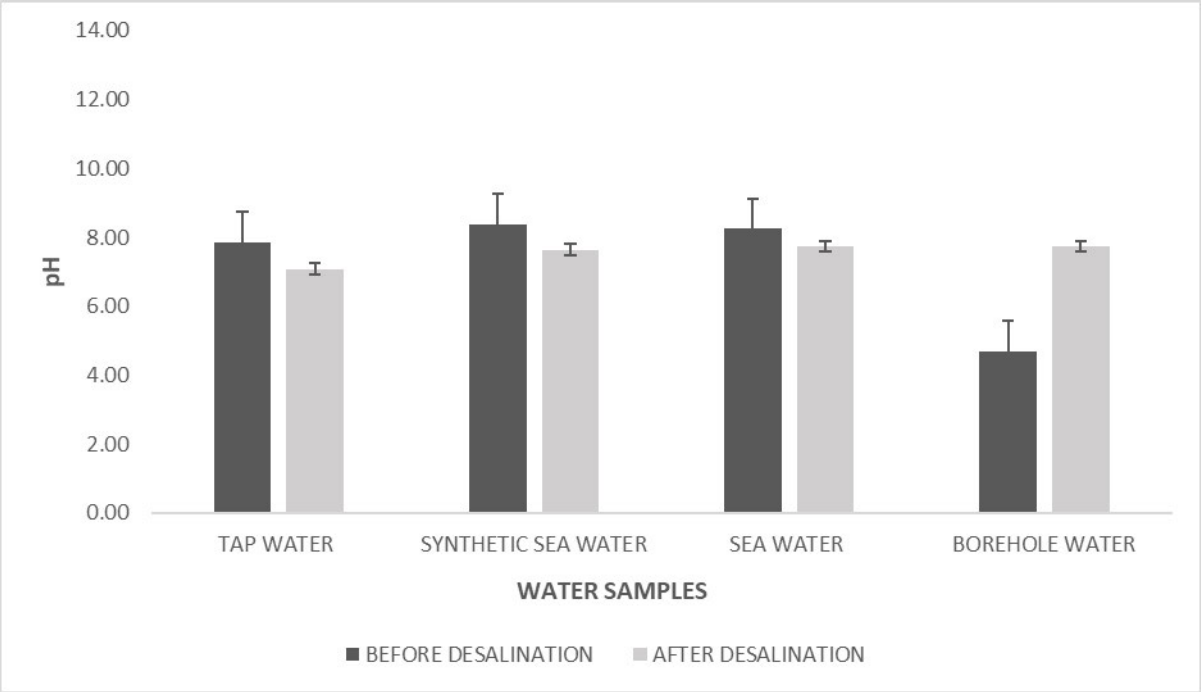

Figure 4.4: pH values of the tap water, seawater, synthetic water and borehole water samples before and after desalination

From figure 4.4, it could be seen that the pH of tap water before and after desalination are deemed suitable for drinking and that of synthetic water and seawater stabilized towards neutral. The recorded pH of borehole water before desalination was 4.67 thus rendering it acidic and deeming it unsuitable for drinking. After desalination, it normalized to 7.74. Before desalination, the sampled tap water was fit for drinking but all others were unfit. After desalination, all of the four water samples became fit for drinking as they ranged between 6.5-8.5 which is the World Health Organizations (WHO) standard for drinking water.

4.5.2 Electrical Conductivity

The electrical conductivity was measured using Mettler Toledo Seven Excellence S470 pH/conductivity meter. Figure 4.5 is a graphical representation of the electrical conductivity values of the water samples before and after desalination. Before desalination, the values for tap water, synthetic water, seawater, and borehole water were 0.8, 237.1, 203, and 52.85 µS/cm respectively while after desalination, the values became 0.2, 0.8, 0.3, and 0.3 µS/cm respectively.

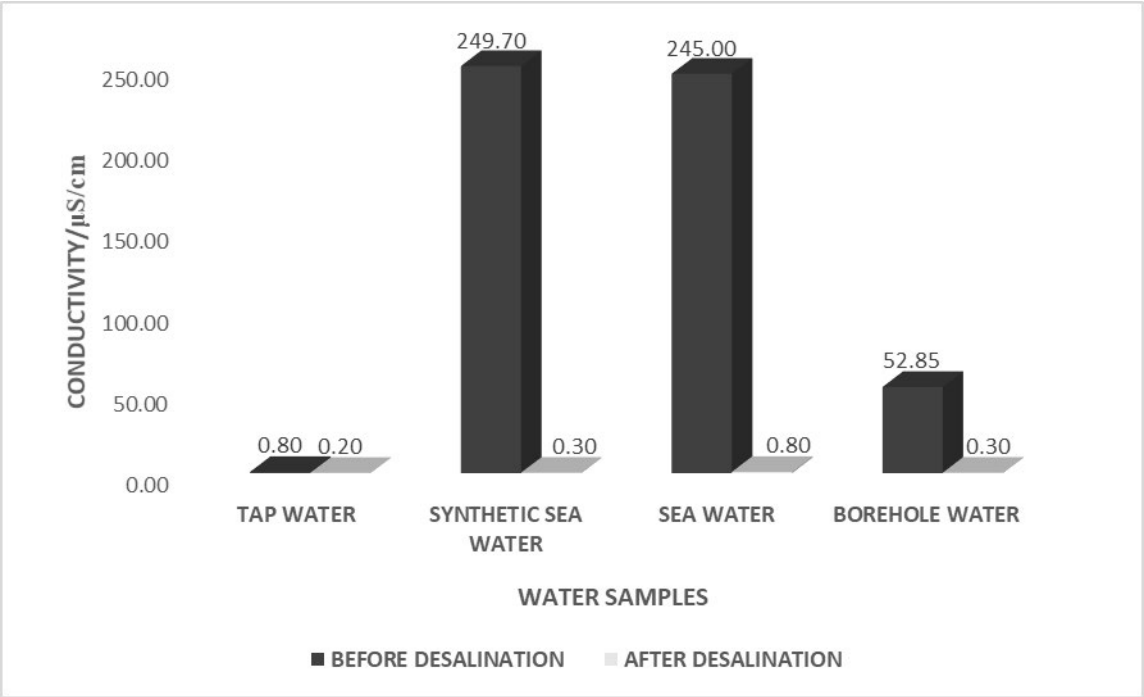

Figure 4.5: Electrical conductivity values of the tap water, seawater, synthetic water and borehole water samples before and after desalination

From Figure 4.5, the conductivity of synthetic water and seawater are seen to generate the highest conductivity readings in comparison to borehole and tap water as expected. This is mainly attributed to the concentration of dissolved salts contained in the water samples. After desalination, the conductivity of the water samples decreased significantly. According to the WHO standard, the standard limit for conductivity in drinking water is 400 µS/cm while the standard limit according to SANS 241 is ≤ 170.

4.5.3 Total Dissolved Solids (TDS)

The values for tap water, synthetic water, seawater and borehole water were 40, 24280, 20680, and 52720 ppm respectively. These values are as a result of the dissolved organic and inorganic materials such as minerals and ions in the water sample. Figure 4.6 is a graphical representation of the TDS values of the water samples before and after desalination. After desalination, the value remained 40 for tap water, and dropped to 120, 80, and 45120 for synthetic water, seawater, and borehole water respectively.

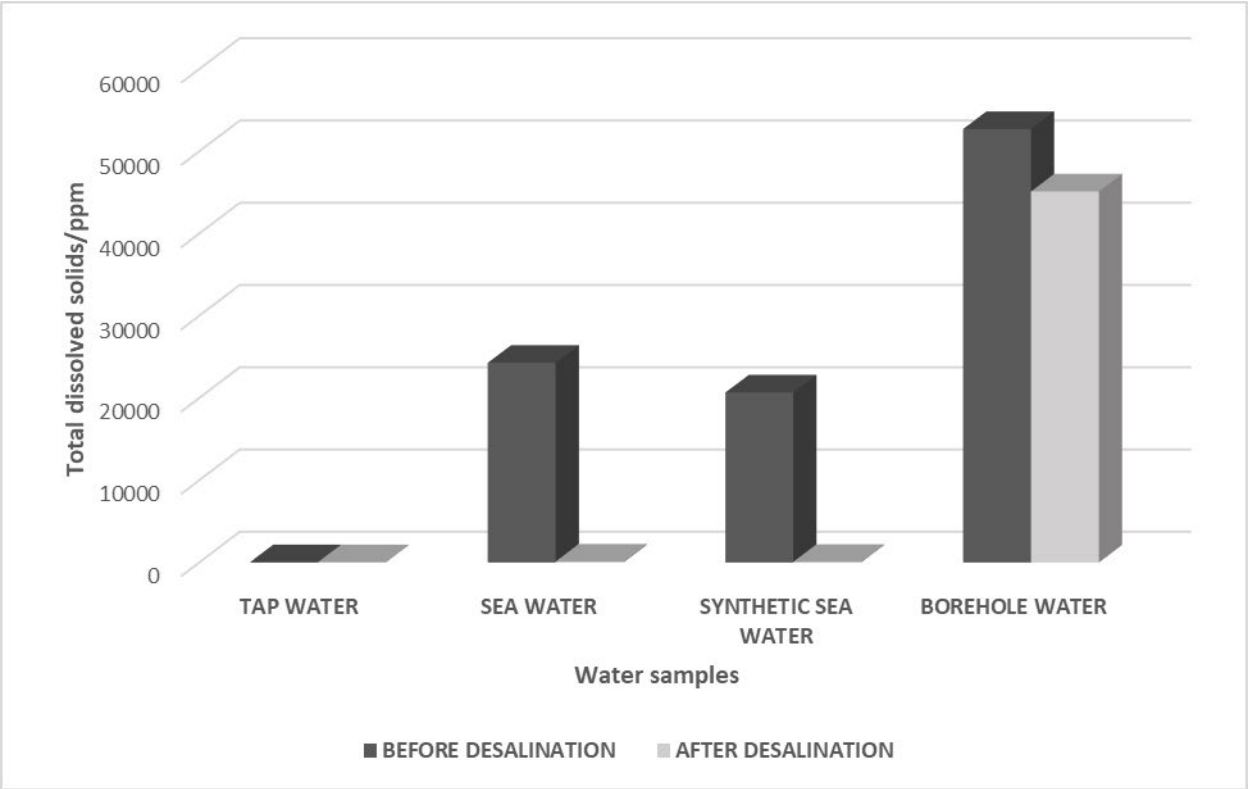

Figure 4.6: TDS values of the tap water, seawater, synthetic water and borehole water samples before and after desalination

From Figure 4.6, the total dissolved solids in the water samples were reduced after desalination. The TDS of tap water before and after desalination is acceptable for drinking. That of seawater and synthetic water before desalination is unacceptable for drinking as the values exceed the permissible limit, while the values gotten after desalination is good and acceptable for drinking. The high value of the borehole water after desalination could be attributed to experimental error. The limit of total dissolved solids is 500-1000 mg/L according to the WHO and according to SANS241 $\leq$ 1200 mg/L.

4.5.4 Salinity

The salinity of the water samples was measured using RS232 Conductivity/Salinity meter AZ 8306. The values for tap water, synthetic water, seawater and borehole water were 2, 30.6, 25.5, and 6.4 ppt, respectively as shown in figure 4.7. After desalination, all the values became approximately 2 ppt. Before desalination, the salinity of tap water and borehole water were relatively low while the salinity of synthetic water and seawater was high. After desalination, the salinity dropped.

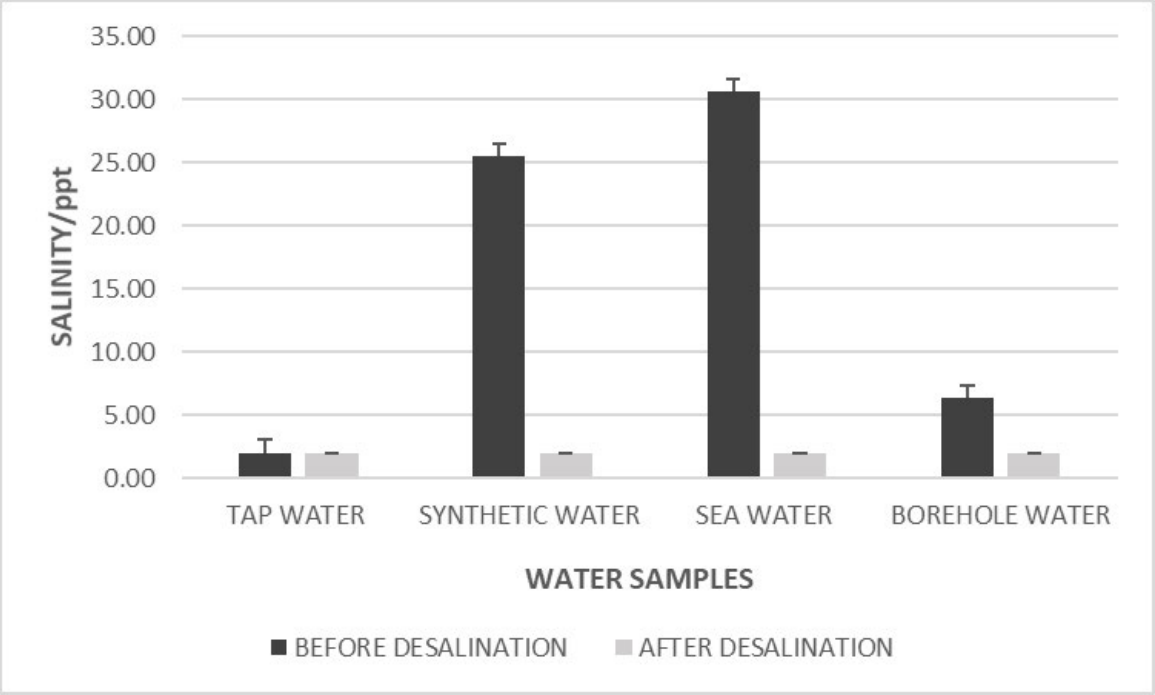

Figure 4.7: Salinity values of the tap water, seawater, synthetic water and borehole water samples before and after desalination

4.6 Scanning electron microscopy (SEM) showing micrographs of cellulose, tyre dust and tyre dust coated cellulose

The use of SEM has been an extremely useful tool in elucidating the structure of the wicking agents used in the solar stills. The micrographs in figure 4.8 have given a clear indication of the variation in the physical structure where (a) is seen to have microfibers arranged in disordered positions while (b) is the tyre dust powder evenly spread. (c) is the cellulose underneath and the tyre dust paint coated on it.

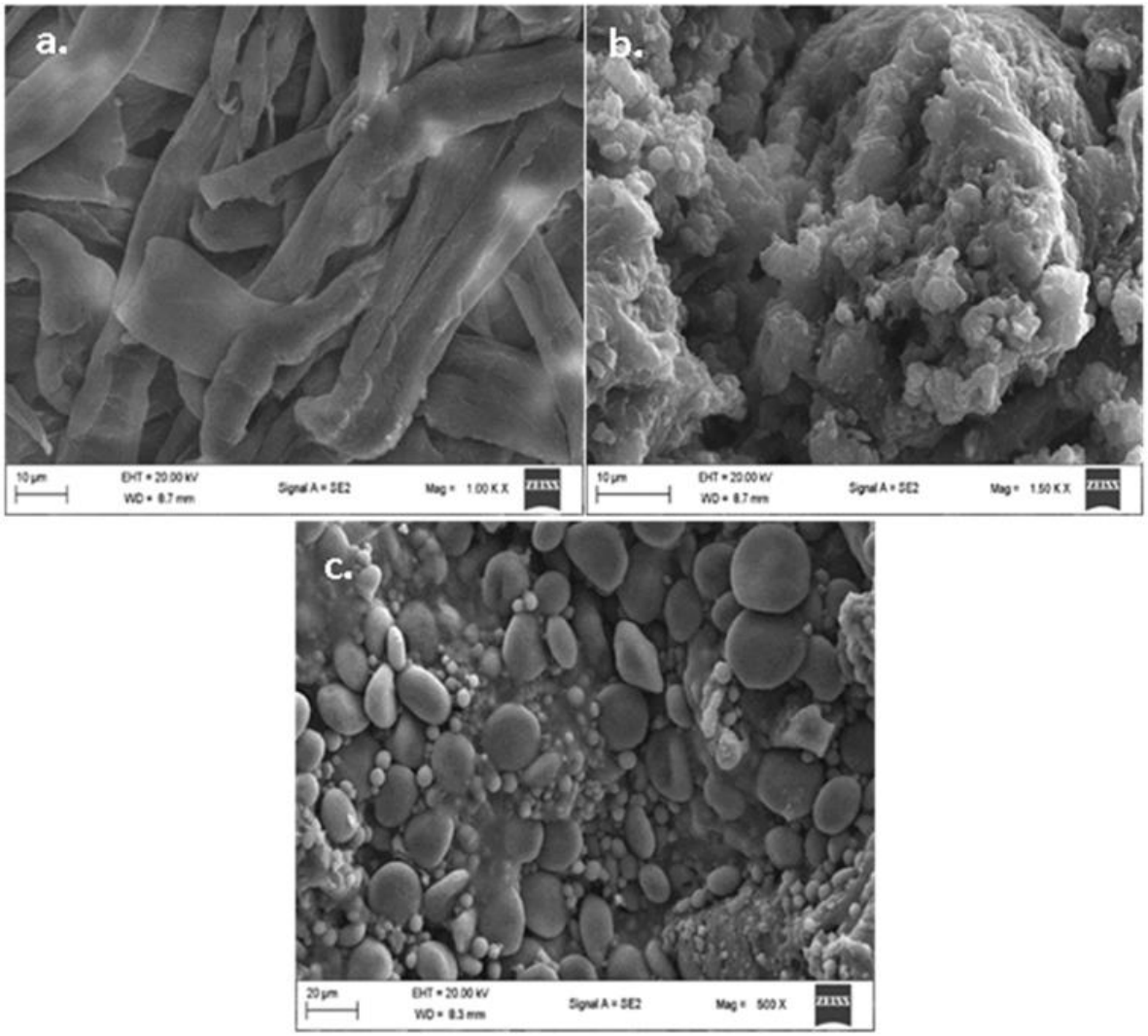

Figure 4.8: Scanning electron microscopy (SEM) photograph of (a) cellulose, (b) tyre dust powder, and (c) tyre dust coated cellulose.

Image (a) shows elongated fibres of cellulose while (b) shows spherical clustered structures of the tyredust powder. From figure (c) which is the cellulose coated with tyre dust, it can be seen that a new surface was created which is a loose and large spherical stone-like structures which seems porous in nature presenting a larger surface area.

4.7 FTIR spectra of cellulose, tyre dust, tyredust paint, and tyre dust coated cellulose

FTIR was employed to analyse the chemical composition and functional groups on the surfaces of CEL, TD PD, TD PNT, and TD CEL which stands for the cellulose board, tyre dust powder, tyre dust paint, and tyre dust coated cellulose. From figure 4.9, it can be seen that the broad bands at 3325, 3344, and 3275 cm^{-1} are attributed to the O-H stretching vibration mode of cellulose in CEL (which indicates the hydrophilic property of cellulose), TD PNT, and TD CEL respectively, with TD PD showing no OH group.

The bands at 1426, 1420, and 1424 cm^{-1} in CEL, TD and TD_CEL respectively were related to carboxylic O-H bending. The bands at 1315 and 1359 cm^{-1} in CEL and TD CEL were related to O-H bending. The band at 1201 cm^{-1} in CEL was related to C-O stretching. The band at 1537 cm^{-1} in TD CEL was assigned to N-O stretching of N-H in plane bending vibration.

The bands at 2100 cm^{-1} show an affinity between the cellulose and TD paint by Hydrogen bonding.

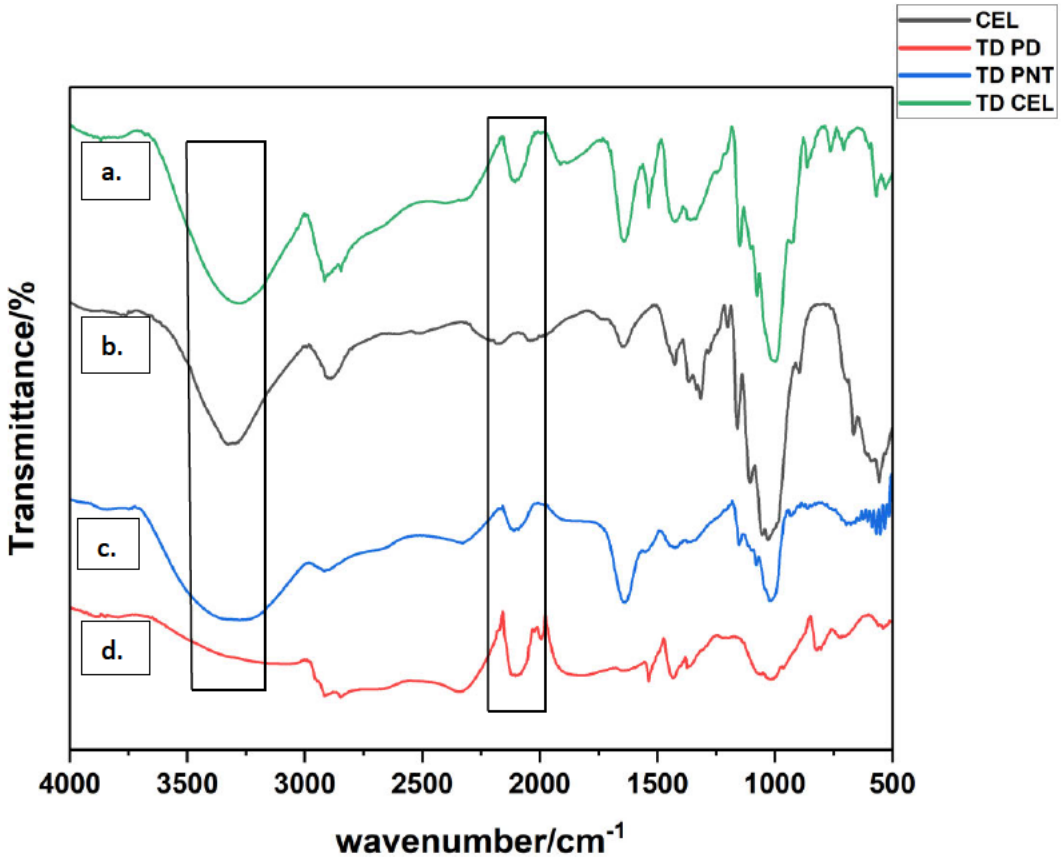

Figure 4.9: Fourier transform infrared spectroscopy (FTIR) spectra of: (a) tyre dust coated cellulose (b) cellulose (c) tyre dust paint (d) tyre dust powder.

4.8 Solar-vapour performance

An outdoor experiment was carried out using the evaporation structure. The mass of the water, the water basin, and the evaporation structure were monitored using Adamdu 75H GFK digital balance to ascertain the rate at which vapor was generated.

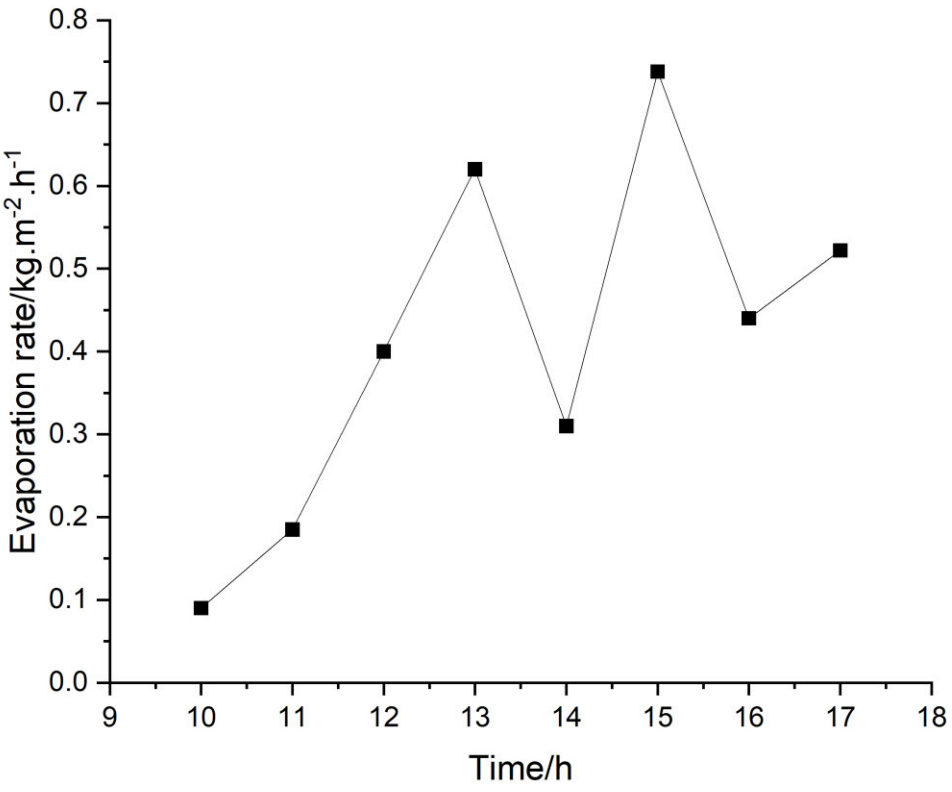

Figure 4.10: The rate of evaporation with time on a sunny day during summer.

From Figure 4.10, the rate of evaporation increased with the intensity of the sun, the intensity of the sun increased at 13:00 and 15:00 which gave rise to the high evaporation rates of 0.62 and 0.738 $kg.m^{-2}.h^{-1}$. The drop in the rate of evaporation has to do with the weather fluctuations during the day which leads to an unsteady weather pattern with the increase and decrease of the sun's intensity. From this, it can be ascertained that the higher the intensity of the sun over time, the higher the rate of evaporation. Therefore, the sun's intensity greatly affects the yield and efficiency of the solar still.

4.9 Temperature proof of interfacial evaporation

During the process of desalination, the temperatures of the black solar absorber (T4), underneath the solar absorber (T3), inside the wicking structure (T2), and the bulk water (T1) were measured using temperature sensors and recorded.

As shown in figure 4.11, It was observed that the temperatures of the solar absorber, T4 and the temperature underneath the solar absorber, T3 increased rapidly from 8:25 a.m. to 12:25 p.m. (mid-day) and started to drop but still remained higher than the temperature of the wick, T2 and bulk water, T1. The temperature of the wicking structure showed an increase and dropped as well while the temperature of the bulk water gradually increased but remained at a much lower temperature slightly above room temperature, and this was a result of the EPS used as an insulating structure.

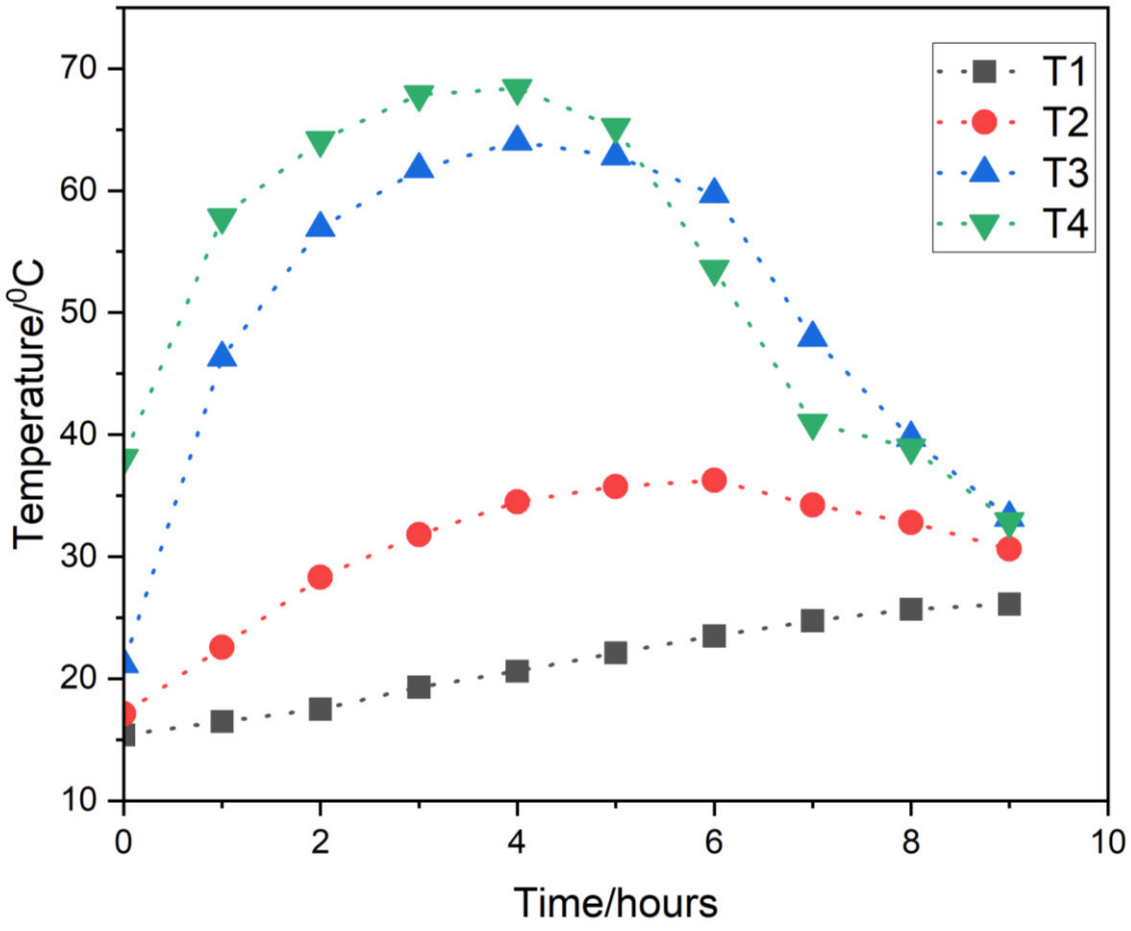

Figure 4.11: Plot showing the temperatures at different locations in the solar still

From this experiment, it can be seen that the insulation material played an optimum role by preventing the bulk water from heating up, thereby increasing interfacial evaporation.

4.10 Metal analysis of tap water, seawater, synthetic water, and borehole water samples before and after desalination

The metal analysis performed on the water samples using ICP-OES gave a visible difference between water samples before desalination and after desalination as shown in figures 4.12, 4.13, 4.14, and 4.15. The metal concentrations were all seen to be higher in the samples before desalination, and after desalination, there were drops in the concentrations of the metals.

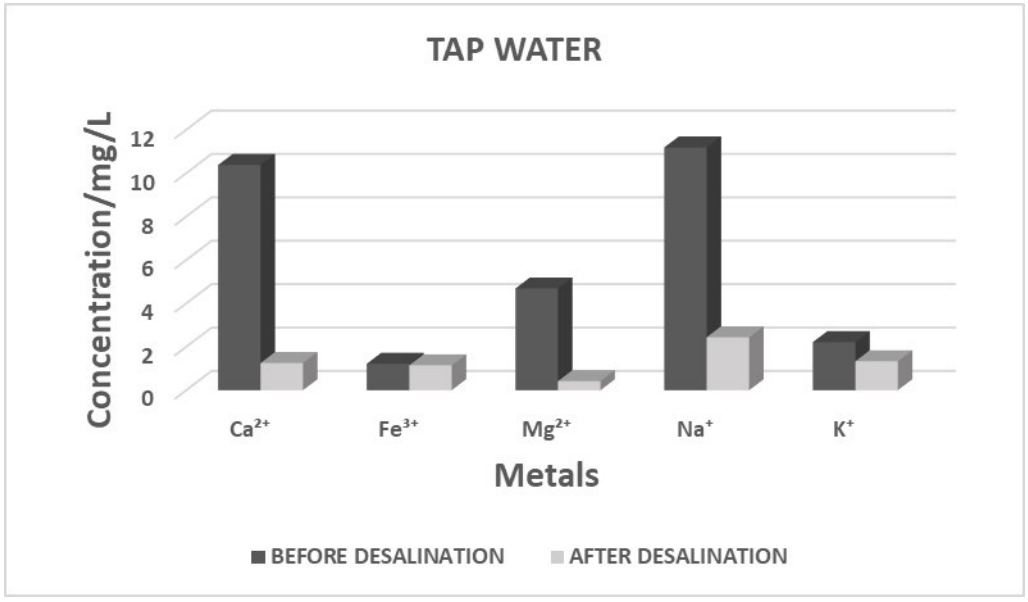

Figure 4.12: Concentration of Ca^{2+}, Fe^{3+}, Mg^{2+}, Na^{+}, and K^{+} in tap water sample before and after desalination

The average concentration of Ca^{2+}, Fe^{3+}, Mg^{2+}, Na^{+}, and K^{+} in tap water as shown in Figure 4.12, before desalination were 10.38, 1.22, 4.69, 11.19, and 2.22 mg/L respectively while after desalination the values dropped to 1.26, 1.15, 0.42, 2.44, and 1.33 mg/L respectively. All of the concentrations before desalination were within the permissible limits according to the WHO and SANS 241 except for iron. After desalination, the values became far below the limit.

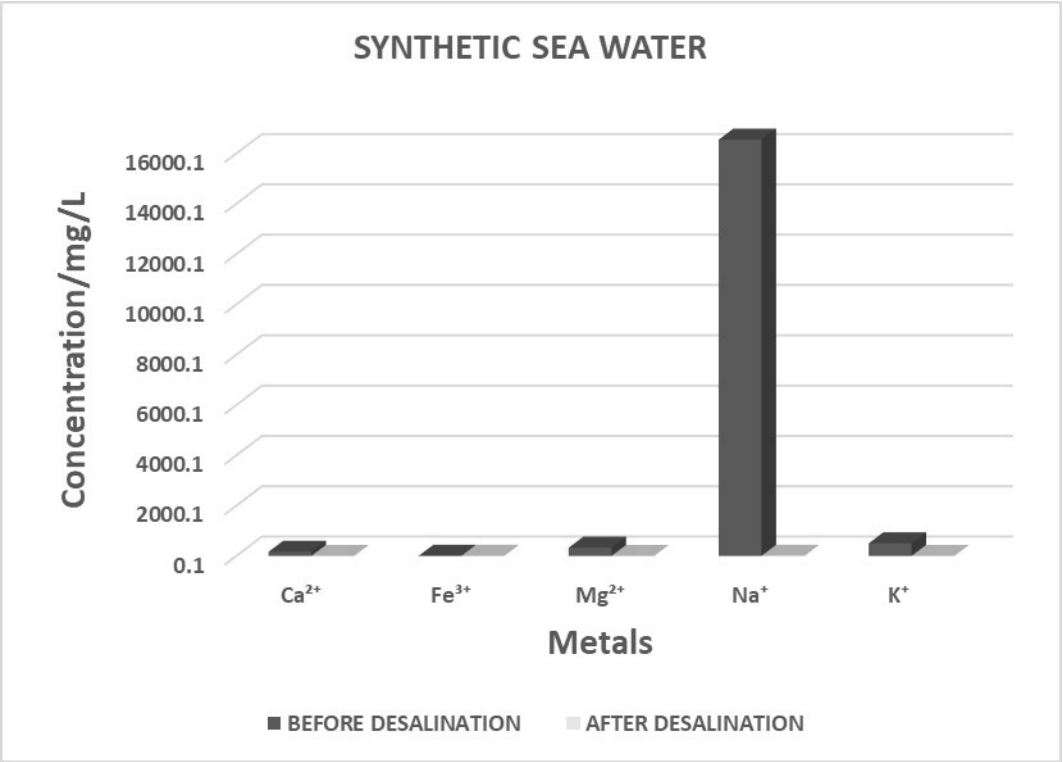

Figure 4.13: Concentration of Ca^{2+}, Fe^{3+}, Mg^{2+}, Na^{+}, and K^{+} in synthetic water sample before and after desalination

For synthetic water sample as shown in Figure 4.13, the average concentration of Ca, Fe, Mg, Na, and K before desalination were 164.33, 1.17, 325.90, 16547.13, and 503.82 mg/L and after desalination, the concentrations became 0.59, 1.04, 0.57, 4.05, and 0.43 mg/L.

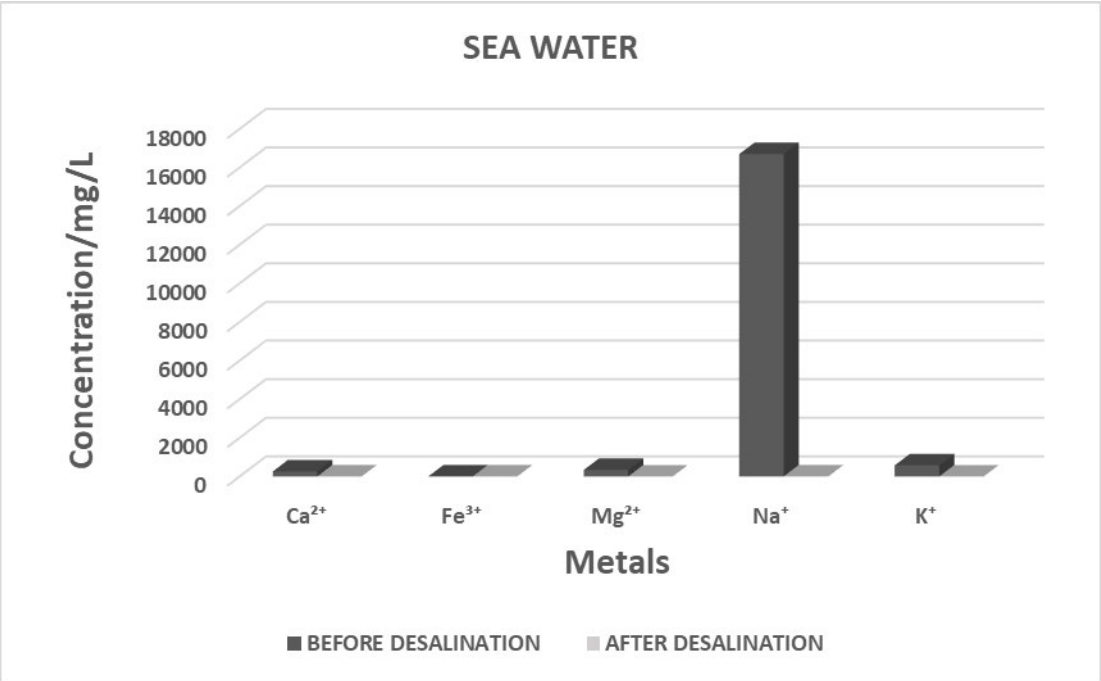

Figure 4.14: Concentration of Ca^{2+}, Fe^{3+}, Mg^{2+}, Na^{+}, and K^{+} in seawater sample before and after desalination

In seawater as shown in figure 4.14, the concentrations of Ca^{2+}, Fe^{3+}, Mg^{2+}, Na^{+}, and K^{+} before desalination were 264.16, 2.63, 341.71, 16699.79, and 581.47 mg/L while after desalination, the average concentrations became 1.67, 1.12, 0.62, 4.30, and 0.50 mg/L.

From the synthetic water and the seawater, the values before desalination were far beyond the limits and are not potable. After desalination, the concentrations dropped massively. This proves that the desalination technique was effective in lowering the concentration of metals in the water samples.

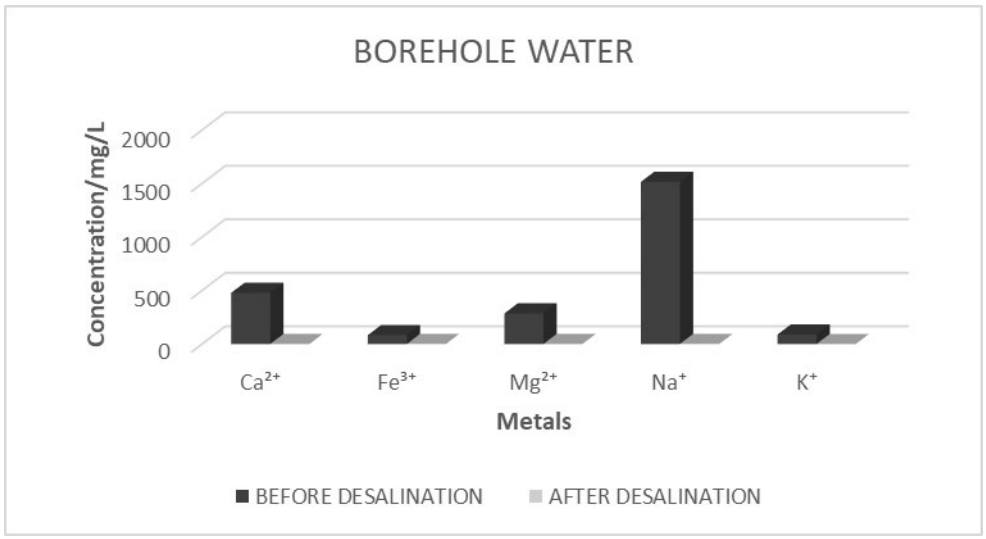

Figure 4.15: Concentration of Ca^{2+}, Fe^{3+}, Mg^{2+}, Na^{+}, and K^{+} in borehole water sample before and after desalination

The average concentration of Ca^{2+}, Fe^{3+}, Mg^{2+}, Na^{+}, and K^{+} in borehole before desalination were 478.58, 83.85, 286.78, 1516.37, and 89.11 mg/L while after desalination, the values became 0.73, 1.27, 0.66, 1.22, and 0.28 mg/L. There is also a massive drop in the concentrations of the metals in borehole water after desalination. This is a scientific proof that desalination using a solar still is effective in lowering the concentration of metals in the water samples.

Reference

WHO. Hardness in drinking water. Background Document for Development of WHO Guidelines for Drinking-Water Quality; World Health Organization: Geneva, Switzerland, 2011; Volume 2.

Chapter 5
Conclusion, Contribution and Recommendations

5.1 Conclusion

The hypothesis stated in Section 1.3 was experimentally proven. The study evidently showed that desalination through the use of a solar still and interfacial evaporation is a sustainable method of water purification that is both cost-effective and highly efficient. This finding not only corroborates with similar studies (e.g Sharon & Reddy 2015; Essa et al., 2022; Shatilla 2020), but also serves as a template on how to popularise the cost-effective water purification among low-income households and communities. The innovative feature of this approach is the use of recycled and cheap materials in providing an efficient method of desalination. Another great advantage is that it utilizes solar energy and was carried out as an outdoor experiment which gives an actual or real-life scale result.

To test the hypothesis, the study aim and objective in Section 1.4 sought to design a sustainable, green, and cost-effective method of water desalination using solar-driven interfacial evaporation. To this effect, A solar still for solar-driven interfacial evaporation desalination with dimension 550 mm x 550 mm was successfully designed and constructed. Also the use of cellulose, tyre dust, polystyrene, and wheat flour to fabricate solar absorber was among the key innovations of this study.

5.2 Summary of Contributions

There are three major contributions of this study which mirror the objectives set out in Section 1.4. The first contribution of the study is the design and construction of a low-cost and efficient solar still for water purification and desalination, and made use of recyclable materials readily available at little or no cost. This specifically responds to Sharon and Reddy (2015) who call for research inot low-cost water purification in developing countries as a solution to potable water crisis.

The second contribution is in line with the second objective which focused on how to advance the throughput volume of the solar still and subsequent ouptput volume of freshwater. The evaporation structure designed exhibited a long-term efficiency of continuous wicking up of water and evaporation even after crystallization on the surface of the absorber. The high desalination performance of the evaporation structure can be ascribed

to the effective heat localisation of the Expanded Polystyrene (EPS), the sufficient water supply of the cellulose as a wicking structure, and the efficiency of the tyre dust coated cellulose that acts as the black solar absorber. An evaporation rate of 0.74 $kg/m^2/h^{-1}$ was achieved from the designed evaporation structure.

In line with the third objective, this study analysed the remediated water obtained from the still. Tap water, seawater, synthetic water, and borehole water were successfully desalinated using the solar still. Physicochemical analysis, metal analysis, and water hardness tests were performed on the water samples before and after desalination. The physicochemical properties of the water samples after desalination showed a reduction in chemical constituents. The pH of the water samples normalized, the electrical conductivity, TDS, and salinity reduced drastically. The water hardness and the metals in them also reduced. Every test carried out proved that solar distillation purifies water that has standard parameters stipulated by the WHO and SANS 241.

Other contributions of the study includes environmental sustainability through the reuse of recyclable materials for water purification. Through the use of recyclable materials and home construction of solar still, this study is an exemplar innovation that will operationalise and expand access to water purification and in turn assist in the attainment of SDGs 6, on drinking water, and to an extent SDG 11, sustainable cities and communities (United Nations 2015). This study offers a practicable solution to the global problem of portable water scarcity and environmental pollution by showing how to increase access to water purification to vulnerable households and communities at an affordable, viable, efficient and sustainable rate. Through the use of different water samples that were purified, the study further demonstrates that individuals and household can replicate same with water sample available to them. By using recyclable materials in the fabrication of the solar still and evaporation structure, this study not only contributes to literature on desalination, but also demonstrates the nexus between environmental sustainability and water treatment.

5.3 Recommendations

A number of recommendations emanate from the study findings and contributions. The study recommends that solar stills of this nature and design can be piloted among low-income households in rural areas and urban areas where potable water scarcity persists. This can

definitely assist in reducing the increasing demand of potable water as a result of population growth. Solar still as an efficiently, low-cost water purification could be among a plathora of solution to drinking water challenging that remains an issue in developing countries.

Further research is urgently needed on how to improve the evaporation rate and yield of the solar still, and this should be funded and encouraged by water regulatory bodies and management as this this will lead to construction of community-scaled solar still to provide potable water at community level. The urgency of this research is because less than six years is left to actualise SDG 6.

Further innovative research is necessary in finding new materials for the construction of the solar stills, for example replacing the pine wood with molded plastic. This would improve the durability and efficiency of the solar still. Future research need to explore the nexus between solar still construction and use of recyclable materials. In other words, the relationship between solar still construction and environmental sustainability in terms of less energy use and recyclable materials remain a niche deserving exploration.

References

Essa, F. A., Abdullah, A. K., Majdi, H. S., Basem, A., Dhahad, H. A., Omara, Z. M., Mohammed, S. A., Alawee, W. H., Ezzi, A. Al, & Yusaf, T. (2022). Parameters Affecting the Efficiency of Solar Stills—Recent Review. *Sustainability (Switzerland)*, *14*(17). https://doi.org/10.3390/su141710668.

Sharon, H., & Reddy, K. S. (2015). A review of solar energy driven desalination technologies. *Renewable and Sustainable Energy Reviews*, *41*, 1080–1118. https://doi.org/10.1016/j.rser.2014.09.002.

Tiwari, G.N., Sahota, L. (2017). *Advanced solar-distillation systems: basic principles, thermal modelling, and its application.* Springer nature Singapore. https://doi.org/10.1007/978-981-10-4672-8.

United Nations. (2015). Transforming our world: the 2030 agenda for sustainable development. Washington DC. 21252030 Agenda for Sustainable Development web.pdf (un.org).

WHO. (2023). *Water is a basic human need*. Geneva. https://wholives.org/our-mission/mission/#.

Appendices

Calculation of total, permanent, and temporary hardness of the tap water, seawater, synthetic water, and borehole water samples.

1. Tap water before desalination

Calculation of total hardness

Average volume of EDTA = 0.00235dm^3

C = 0.01 M

n = CV

$(0.01)(0.00235)$ =0.0000235 moles of EDTA

Number of moles of EDTA = moles of $CaCO_3$

Equation of the reaction:

$$CaCO_3 + EDTA^{4-}_{(aq)} \rightarrow Ca(EDTA)^{2-}_{(aq)} + CO_3^{2-}{}_{(aq)}$$

$C_{CaCO3} = {}^{n}/_{v}$

$$= \frac{0.0000235 \text{ moles}}{0.05}$$

= 0.00047 mol/dm^3

Concentration of $CaCO_3$ in mg/L:

= 0.00047 mol/dm^3 x 100.0869 g/mol x 1000

= 47.041 mg/L (Total hardness of tap water sample before desalination)

Calculation of permanent and temporary hardness

Average volume of EDTA = 0.0023 dm^3

C = 0.01 M

n = CV

$(0.01)(0.0023)$ =0.000023 moles

Number of moles of EDTA = moles

Equation of the reaction:

$$CaCO_3 + EDTA^{4-}_{(aq)} \rightarrow Ca(EDTA)^{2-}_{(aq)} + CO_3^{2-}{}_{(aq)}$$

Therefore, number of moles of $CaCO_3$, nCaCO3 = moles

$C_{CaCO3} = {}^{n}/_{v}$

$$= \frac{0.000023 \text{ moles}}{0.05}$$

$= 0.00046$ mol/dm^3

Concentration of $CaCO_3$ in mg/L:

= 0.00046 mol/dm^3 x 100.0869 g/mol x 1000

= 46.040 mg/L (Permanent hardness of tap water sample before desalination)

Temporary hardness = Total hardness – permanent hardness

47.041 mg/L - 46.040 mg/L

= 1.0008 mg/L (Temporary hardness of tap water sample before desalination)

2. Tap water sample after desalination

Total hardness

Average volume of EDTA = 0.0004 dm^3

C = 0.01 M

n = CV

$(0.01)(0.0023)$ =0.000004 moles

Number of moles of EDTA = moles

Equation of the reaction:

$$CaCO_3 + EDTA^{4-}_{(aq)} \rightarrow Ca(EDTA)^{2-}_{(aq)} + CO_3^{2-}{}_{(aq)}$$

Therefore, number of moles of $CaCO_3$, nCaCO3 = moles

$C_{CaCO3} = {}^{n}/_{v}$

$= \frac{0.000004 \text{ moles}}{0.05}$

= 0.00008 mol/dm^3

Concentration of $CaCO_3$ in mg/L:

= 0.00008 mol/dm^3 x 100.0869 g/mol x 1000

= 8.0070 mg/L (Total hardness of tap water sample after desalination)

Permanent and temporary hardness

On addition of EBT, purple colour was observed.

Average volume of EDTA = 0.00035 dm^3

C = 0.01 M

n = CV

$(0.01)(0.00035)$ =0.0000035 moles

Number of moles of EDTA = moles

Equation of the reaction:

$$CaCO_3 + EDTA^{4-}_{(aq)} \rightarrow Ca(EDTA)^{2-}_{(aq)} + CO^{2-}_{3\ (aq)}$$

Therefore, number of moles of $CaCO_3$, nCaCO3 = moles

$C_{CaCO3} = {}^{n}/_{v}$

$= \frac{0.0000035 \text{ moles}}{0.05}$

= 0.00007 mol/dm^3

Concentration of $CaCO_3$ in mg/L:

= 0.00007 mol/dm^3 x 100.0869 g/mol x 1000

= 7.006 mg/L (Permanent hardness of tap water sample after desalination)

Temporary hardness = Total hardness – permanent hardness

8.006952 mg/L - 7.006mg/L

= 1.000852 mg/L (Temporary hardness of tap water sample after desalination)

3. Seawater sample before desalination

Total hardness

Seawater sample before desalination: A hundred times dilution was done on the sample before titrating with EDTA.

Average volume of EDTA = 0.00328dm^3

C = 0.01 M

n = CV

$(0.01)(0.00328)$ =0.0000328 moles of EDTA

Number of moles of EDTA = moles of $CaCO_3$

Equation of the reaction:

$$CaCO_3 + EDTA^{4-}_{(aq)} \rightarrow Ca(EDTA)^{2-}_{(aq)} + CO_3^{2-}{}_{(aq)}$$

$C_{CaCO3} = {}^{n}/_{v}$

$$= \frac{0.0000328 \text{ moles}}{0.05}$$

= 0.000656 mol/dm^3

Concentration of $CaCO_3$ in mg/L:

= 0.000656 mol/dm^3 x 100.0869 g/mol x 1000

= 65.6570 mg/L x 100(dilution)

= 6565.70 mg/L (Total hardness of seawater sample before desalination)

Permanent and temporary hardness

Average volume of EDTA = 0.003133 dm^3

C = 0.01 M

n = CV

$(0.01)(0.003133)$ =0.00003133 moles

Number of moles of EDTA = moles

Equation of the reaction:

$$CaCO_3 + EDTA^{4-}_{(aq)} \rightarrow Ca(EDTA)^{2-}_{(aq)} + CO^{2-}_{3\ (aq)}$$

Therefore, number of moles of $CaCO_3$, nCaCO3 = moles

$C_{CaCO3} = {}^{n}/_{v}$

$$= \frac{0.00003133 \text{ moles}}{0.05}$$

$= 0.0006267$ mol/dm^3

Concentration of $CaCO_3$ in mg/L:

= 0.0006267 mol/dm^3 x 100.0869 g/mol x 1000

= 62.7210 mg/L x 100 (dilution)

= 6272.106 mg/L (Permanent hardness of seawater sample before desalination)

Temporary hardness = Total hardness – permanent hardness

6565.701 mg/L – 6272.106 mg/L

= 293.595 mg/L (Temporary hardness of seawater sample before desalination)

1 Seawater after desalination

Total hardness

Average volume of EDTA = 0.0008 dm^3

C = 0.01 M

n = CV

$(0.01)(0.0008)$ =0.000008 moles of EDTA

Number of moles of EDTA = moles of $CaCO_3$

Equation of the reaction:

$$CaCO_3 + EDTA^{4-}_{(aq)} \rightarrow Ca(EDTA)^{2-}_{(aq)} + CO^{2-}_{3\ (aq)}$$

$C_{CaCO3} = {}^{n}/_{v}$

$$= \frac{0.000008 \text{ moles}}{0.05}$$

= 0.00016 mol/dm^3

Concentration of $CaCO_3$ in mg/L:

= 0.00016 mol/dm^3 x 100.0869 g/mol x 1000

= 16.0139 mg/L (Total hardness of seawater sample after desalination)

Permanent and temporary hardness

Average volume of EDTA = 0.00065 dm^3

C = 0.01 M

n = CV

$(0.01)(0.00065)$ =0.0000065 moles

Number of moles of EDTA = moles of $CaCO_3$

Equation of the reaction:

$$CaCO_3 + EDTA^{4-}_{(aq)} \rightarrow Ca(EDTA)^{2-}_{(aq)} + CO_3^{2-}{}_{(aq)}$$

Therefore, number of moles of $CaCO_3$, nCaCO3 = moles

$C_{CaCO3} = {}^{n}/_{v}$

$$= \frac{0.0000065 \text{ moles}}{0.05}$$

= 0.00013 mol/dm^3

Concentration of $CaCO_3$ in mg/L:

= 0.00013 mol/dm^3 x 100.0869 g/mol x 1000

= 13.011 mg/L (Permanent hardness of seawater sample after desalination)

Temporary hardness = Total hardness – permanent hardness

16.0139 mg/L – 13.011 mg/L

= 3.003 mg/L (Temporary hardness of seawater sample after desalination)

2 Synthetic water before desalination

Total hardness

Average volume of EDTA = 0.0031 dm^3

C = 0.01 M

n = CV

$(0.01)(0.0031)$ =0.000031 moles

Number of moles of EDTA = moles of $CaCO_3$

Equation of the reaction:

$$CaCO_3 + EDTA^{4-}_{(aq)} \rightarrow Ca(EDTA)^{2-}_{(aq)} + CO_3^{2-}{}_{(aq)}$$

Therefore, number of moles of $CaCO_3$, $nCaCO_3$ = moles

$C_{CaCO3} = {}^{n}/_{v}$

$$= \frac{0.000031 \text{ moles}}{0.05}$$

= 0.00062 mol/dm^3

Concentration of $CaCO_3$ in mg/L:

= 0.00062 mol/dm^3 x 100.0869 g/mol x 1000

= 62.0539 mg/L x 100 (dilution)

= 6205.39 mg/L (Total hardness of synthetic water sample before desalination)

Permanent and temporary hardness

Average volume of EDTA = 0.002775 dm^3

C = 0.01 M

n = CV

$(0.01)(0.002775)$ =0.00002775 moles

Number of moles of EDTA = moles of $CaCO_3$

Equation of the reaction:

$$CaCO_3 + EDTA^{4-}_{(aq)} \rightarrow Ca(EDTA)^{2-}_{(aq)} + CO_3^{2-}{}_{(aq)}$$

Therefore, number of moles of $CaCO_3$, nCaCO3 = moles

$C_{CaCO3} = {}^{n}/_{v}$

$= \frac{0.00002775 \text{ moles}}{0.05}$

$= 0.000555 \text{ mol/dm}^3$

Concentration of $CaCO_3$ in mg/L:

$= 0.000555 \text{ mol/dm}^3 \times 100.0869 \text{ g/mol} \times 1000$

= 55.548 mg/L x 100 (dilution)

= 5554.823 mg/L (Permanent hardness of synthetic water sample before desalination)

Temporary hardness = Total hardness – permanent hardness

6205.39 mg/L – 5554.823 mg/L

= 650.567 mg/L (Temporary hardness of synthetic water sample before desalination)

3 Synthetic water after desalination

Average volume of EDTA = 0.0002 dm^3

C = 0.01 M

n = CV

$(0.01)(0.0031)$ =0.000002 moles

Number of moles of EDTA = moles of $CaCO_3$

Equation of the reaction:

$$CaCO_3 + EDTA^{4-}_{(aq)} \rightarrow Ca(EDTA)^{2-}_{(aq)} + CO_3^{2-}{}_{(aq)}$$

Therefore, number of moles of $CaCO_3$, nCaCO3 = moles

$C_{CaCO3} = {}^{n}/_{v}$

$= \frac{0.000002 \text{ moles}}{0.05}$

$= 0.00004 \text{ mol/dm}^3$

Concentration of $CaCO_3$ in mg/L:

= 0.00004 mol/dm^3 x 100.0869 g/mol x 1000

= 4.0035 mg/L (Total hardness of synthetic water sample after desalination)

Permanent and temporary hardness

Average volume of EDTA = 0.000125 dm^3

C = 0.01 M

n = CV

$(0.01)(0.000125)$ =0.00000125 moles

Number of moles of EDTA = moles of $CaCO_3$

Equation of the reaction:

$$CaCO_3 + EDTA^{4-}_{(aq)} \rightarrow Ca(EDTA)^{2-}_{(aq)} + CO^{2-}_{3\ (aq)}$$

Therefore, number of moles of $CaCO_3$, nCaCO3 = moles

$C_{CaCO3} = {}^{n}/_{v}$

$$= \frac{0.00000125 \text{ moles}}{0.05}$$

= 0.000025 mol/dm^3

Concentration of $CaCO_3$ in mg/L:

= 0.000025 mol/dm^3 x 100.0869 g/mol x 1000

= 2.502 mg/L (Permanent hardness of synthetic water sample after desalination)

Temporary hardness = Total hardness – permanent hardness

4.0035 mg/L – 2.502 mg/L

= 1.5015 mg/L (Temporary hardness of synthetic water sample after desalination)

4 Borehole water sample before desalination

Total hardness

Average volume of EDTA = 0.00125 dm^3

C = 0.01 M

n = CV

$(0.01)(0.00125)$ =0.0000125 moles

Number of moles of EDTA = moles of $CaCO_3$

Equation of the reaction:

$$CaCO_3 + EDTA^{4-}_{(aq)} \rightarrow Ca(EDTA)^{2-}_{(aq)} + CO_3^{2-}{}_{(aq)}$$

Therefore, number of moles of $CaCO_3$, nCaCO3 = moles

$C_{CaCO3} = {}^{n}/_{v}$

$$= \frac{0.0000125 \text{ moles}}{0.05}$$

= 0.00025 mol/dm^3

Concentration of $CaCO_3$ in mg/L:

= 0.00025 mol/dm^3 x 100.0869 g/mol x 1000

= 25.0217 mg/L x 100 (dilution)

= 2502.1725 mg/L (Total hardness of borehole water sample before desalination)

Permanent and temporary hardness

Average volume of EDTA = 0.0012 dm^3

C = 0.01 M

n = CV

$(0.01)(0.0012)$ =0.000012 moles

Number of moles of EDTA = moles of $CaCO_3$

Equation of the reaction:

$$CaCO_3 + EDTA^{4-}_{(aq)} \rightarrow Ca(EDTA)^{2-}_{(aq)} + CO_3^{2-}{}_{(aq)}$$

Therefore, number of moles of $CaCO_3$, nCaCO3 = moles

$C_{CaCO3} = {}^{n}/_{v}$

$$= \frac{0.000012 \text{ moles}}{0.05}$$

= 0.00024 mol/dm^3

Concentration of $CaCO_3$ in mg/L:

= 0.00024 mol/dm^3 x 100.0869 g/mol x 1000

= 24.021 mg/L x 100 (dilution)

= 2402.1 mg/L (Permanent hardness of borehole water sample before desalination)

Temporary hardness = Total hardness – permanent hardness

2502.1725 mg/L – 2402.1 mg/L

= 100.0725 mg/L (Temporary hardness of borehole water sample before desalination